arXiv:1308.1283v2 [hep-lat] 19 Nov 2013

Ghost sector and geometry in minimal Landau gauge: further constraining the infinite-volume limit

Attilio Cucchieri[1,*] and Tereza Mendes[1,†]

[1] *Instituto de Física de São Carlos, Universidade de São Paulo, Caixa Postal 369, 13560-970 São Carlos, SP, Brazil*

(Dated: October 30, 2021)

We present improved upper and lower bounds for the momentum-space ghost propagator of Yang-Mills theories in terms of the two smallest nonzero eigenvalues (and their corresponding eigenvectors) of the Faddeev-Popov matrix. These results are verified using data from four-dimensional numerical simulations of SU(2) lattice gauge theory in minimal Landau gauge at $\beta = 2.2$, for lattice sides $N =$ 16, 32, 48 and 64. Gribov-copy effects are discussed by considering four different sets of numerical minima. We then present a lower bound for the smallest nonzero eigenvalue of the Faddeev-Popov matrix in terms of the smallest nonzero momentum on the lattice and of a parameter characterizing the geometry of the first Gribov region Ω. This allows a simple and intuitive description of the infinite-volume limit in the ghost sector. In particular, we show how nonperturbative effects may be quantified by the rate at which typical thermalized and gauge-fixed configurations approach the boundary of Ω, known as the first Gribov horizon. As a result, a simple and concrete explanation emerges for why lattice studies do not observe an enhanced ghost propagator in the deep infrared limit. Most of the simulations have been performed on the Blue Gene/P–IBM supercomputer shared by Rice University and São Paulo University.

* attilio@ifsc.usp.br

† mendes@ifsc.usp.br

I. INTRODUCTION

It is well known that the infinite-volume extrapolation of numerical data is a key step to obtain continuum results for minimal-Landau-gauge-fixed Green's functions in Yang-Mills theories (see e.g. [1–3] and references therein). Extracting the relevant infinite-volume information from lattice simulations is, however, a difficult computational task, since analytic results that might guide the necessary extrapolation are still limited. In particular, the main — and widely accepted — assumption governing the infinite-volume limit in minimal Landau gauge is that

> *At very large volumes, the functional integration gets concentrated on the boundary $\partial\Omega$ of the first Gribov region Ω [defined by transverse gauge configurations with all nonnegative eigenvalues of the Faddeev-Popov (FP) matrix $\mathcal{M}(b,x;c,y)$].*

This is explained by considering the interplay among the volume of configuration space, the Boltzmann weight associated to the gauge configurations and the step function used to constrain the functional integration to the region Ω. Indeed, since the configuration space has very large dimensionality, we expect that, for large volumes, entropy will favor configurations near the boundary $\partial\Omega$ of Ω [4, 5]. (For a pictorial visualization of this competition see Figure 2 of Ref. [4] and Figure 3.5 of Ref. [6] or, equivalently, Figure 2.5 of Ref. [7].) The above statement is supported by numerical data: the average value of the smallest nonzero eigenvalue λ_1 of $\mathcal{M}(b,x;c,y)$ goes to zero as the lattice volume increases in 2d [8], 3d [9] and 4d [10] minimal Landau gauge.

These results give rise to a simple picture. For very small physical volumes one expects the measure to be concentrated around $A = 0$, i.e. the lattice configuration should be purely perturbative (see for example [11, 12] for numerical simulations in the perturbative regime). Conversely, for sufficiently large physical volumes, nonperturbative effects (and in particular the confinement mechanism) should be at work. Such effects should be encoded in configurations on and around the boundary of Ω. Thus, if one accepts the above assumption, the functional integration should be strongly dominated at very large volumes by configurations belonging to a thin layer close to $\partial\Omega$. This indeed seems to be the case if one looks at the plots reported on the left column of Figure 1 in Ref. [10] (see also Figures 1 and 2 in Ref. [13]).

At the same time, the study of Green's functions of Yang-Mills theories in minimal Landau gauge is complicated by the existence of Gribov copies [14–16], corresponding to different local minima[1] of the minimizing functional

$$\mathcal{E}[A] \,=\, \int d^d x \, \mathrm{Tr}\left[A^{(g)}_\mu(x)\, A^{(g)}_\mu(x) \right] \,, \tag{1}$$

used to define this gauge (in the continuum). [Here, $A^{(g)}_\mu(x)$ is the gauge-transformed gauge field.] Indeed, at finite volume, different sets of local minima have been shown to yield different results for the numerical data [10, 13, 17–30]. Thus, in the infinite-volume limit, systematic effects due to Gribov copies should be taken into account. With respect to these effects, two different possibilities have been discussed:

- The influence of Gribov copies becomes smaller as the volume increases [23–25]. These results are supported by the analysis carried out in Ref. [31], which showed that the normalized probability distributions over the first Gribov region Ω and over the fundamental modular region Λ — defined [4, 32] by the absolute minima of $\mathcal{E}[A]$ — are equal (in the sense that their moments of finite order are equal).

- Gribov copies should be related to different possible infrared behaviors of minimal-Landau-gauge Green's functions, i.e. different sets of numerical minima — such as those considered in Refs. [13, 28, 33] — would yield qualitatively different results, and these differences would survive the infinite-volume limit. Very recently, in Ref. [34], different infinite-volume results were indeed obtained, for the gluon propagator in the $3d$ SU(2) case, depending on whether the averages were taken in Ω or restricted to Λ.

---

[1] With respect to gauge transformations $\{g(x)\}$.

In Refs. [35, 36] we introduced upper and lower bounds for the gluon[2] and the ghost propagators using a magnetization-like quantity in the former case and the smallest nonzero eigenvalue λ_1 of the FP matrix (and the corresponding eigenvector) in the latter. These bounds allow a better control of the extrapolation of the data to infinite volume [1–3, 35, 36]. They also provide a better intuition of the relevant aspects of the theory as very large lattice sizes N are considered. In particular, in the ghost case, one can show that the inverse of λ_1 is an upper bound for the ghost propagator $G(p)$ [see Eq. (2) in the next section]. As explained above, for very large N, one expects the relevant configurations to be very close to $\partial\Omega$, i.e. these configurations should be characterized by very small values for λ_1. Thus, in order to describe the extrapolation $N \to +\infty$ in the ghost sector, we can re-formulate the above assumption and say that

> *The key point seems to be the rate at which λ_1 goes to zero, which, in turn, should be related to the rate at which a thermalized and gauge-fixed configuration approaches $\partial\Omega$.*

This observation has partially prompted the present work. Indeed, we present here (see Section IV) a lower bound for λ_1 that allows us to give a simple mathematical realization of the above statement.

A relevant aspect of the bounds proven in [36], as well as of the new bounds presented here, is that they apply to any configuration of Ω. As a consequence, they can be used for any Gribov copy of the minimal Landau gauge. Of course, Gribov-copy effects may (or may not) be present also in the quantities entering the formulae of the bounds.[3] On the other hand, the possibility of comparing Gribov-copy effects for several, related, quantities could be useful to understand what triggers these effects and when they are relevant.

The present work is organized as follows. In the next section we review the proof presented in Ref. [36] and we show how the previous bounds can be systematically improved, by considering a larger set of eigenvalues (and eigenvectors) of the FP matrix. These results are numerically verified in Section III. Let us recall that a complete verification of the bounds was lacking in Ref. [36], since in most of our old simulations we did not collect data for the smallest eigenvalues λ_1 or for the corresponding eigenvector. This omission is now rectified, considering SU(2) data at $\beta = 2.2$, for lattice volumes up to 64^4. In Section III we also discuss Gribov-copy effects by considering four different sets of numerical minima. A lower bound for λ_1 is proven in Section IV and numerically verified in Section V, by an unconventional approach. This bound, which is written in terms of the smallest nonzero lattice momentum p_{min} and of a parameter characterizing the geometry of the first Gribov region Ω, implies i) a simple upper bound for the ghost propagator [see Eq. (33) below], ii) a stronger version of the so-called no-pole condition [see Eq. (35)] and iii) a new bound for the so-called horizon function [see Eq. (42)]. It also allows a better understanding of the infinite-volume limit and a simple explanation of some of the results published in the literature (see Section VI). Finally, in Section VII, we present our conclusions.

II. BOUNDS FOR $G(p_{min})$ (OLD AND NEW)

In Ref. [36] (see also [1–3]) we have proven that, in the SU(N_c) case, for any nonzero momentum p and for any gauge-fixed configuration that belongs to the interior of the first Gribov region Ω, the minimal-Landau-gauge ghost propagator $G(p)$ satisfies the bounds

$$\frac{1}{N_c^2-1}\,\frac{1}{\lambda_1}\,\sum_b |\widetilde{\psi}_1(b,p)|^2 \;\leq\; G(p) \;\leq\; \frac{1}{\lambda_1}\,. \tag{2}$$

Here, $b = 1, 2, \ldots, N_c^2 - 1$ is a color index running over the $N_c^2 - 1$ generators of SU(N_c) and $p(k)$ is the lattice momentum, whose components are $p_\mu(k) = 2\sin(\pi k_\mu/N)$ with $k_\mu = 0, 1, \ldots, N-1$, where N is the lattice size.

---

[2] Interesting bounds in the gluon sector have also been recently proven in Refs. [37, 38].

[3] For example, we already know that this is the case for the smallest nonzero eigenvalue λ_1 [10, 18].

We indicate with λ_1 the smallest nonzero eigenvalue of the FP matrix $\mathcal{M}(b,x;c,y)$, with $\psi_1(b,x)$ the corresponding eigenvector and with $\widetilde{\psi}_1(b,p)$ its Fourier transform, for which we use the definition

$$\widetilde{\psi}_i(b,p) \,=\, \frac{1}{\sqrt{V}} \sum_x \psi_i(b,x)\, e^{-2\pi i k\cdot x} \;, \tag{3}$$

where $V = N^d$ is the lattice volume (in the d-dimensional case) and we indicate with $\psi_i(b,x)$ a generic eigenvector of $\mathcal{M}(b,x;c,y)$. These bounds were obtained by considering the equations

$$G(p) \,=\, \frac{1}{N_c^2-1} \sum_{x,\,y,\,b} \frac{e^{-2\pi i\, k\cdot(x-y)}}{V}\, \mathcal{M}^{-1}(b,x;b,y) \,=\, \frac{1}{N_c^2-1} \sum_{i:\lambda_i\neq 0} \sum_b \lambda_i^{-1}\, |\widetilde{\psi}_i(b,p)|^2 \;, \tag{4}$$

valid in the space orthogonal to the kernel of the FP matrix. Then, using the inequalities[4]

$$0 \,<\, \lambda_1 \,<\, \lambda_2 \,<\, \lambda_3 \,\ldots \;, \tag{5}$$

we can write[5]

$$\frac{1}{N_c^2-1}\, \frac{1}{\lambda_1} \sum_b |\widetilde{\psi}_1(b,p)|^2 \,\leq\, G(p) \tag{6}$$

and

$$G(p) \,\leq\, \frac{1}{N_c^2-1}\, \frac{1}{\lambda_1} \sum_{i:\lambda_i\neq 0} \sum_b |\widetilde{\psi}_i(b,p)\,|^2 \;. \tag{7}$$

Thus, after summing and subtracting in Eq. (7) the contributions from the eigenvectors spanning the kernel of $\mathcal{M}(b,x;c,y)$ and using the completeness relation

$$\sum_i \psi_i(b,x)\, \psi_i^*(c,y) \,=\, \delta_{bc}\, \delta_{xy} \;, \tag{8}$$

where * indicates complex conjugation, we find

$$G(p) \,\leq\, \frac{1}{\lambda_1} \left[1 \,-\, \frac{1}{N_c^2-1} \sum_{j:\lambda_j=0} \sum_b |\widetilde{\psi}_j(b,p)\,|^2 \right] \;. \tag{9}$$

In Landau gauge the eigenvectors corresponding to the null eigenvalue are constant modes and, for any nonzero momentum p, we immediately obtain the upper bound in Eq. (2). One should note that the above upper bound becomes an equality if and only if the eigenvalues of the FP matrix are all degenerate and equal to λ_1.

The above result can be (systematically) improved, by considering also the eigenvalues $\lambda_2, \lambda_3, \ldots$ and the inequalities (5). For example, if λ_2 and $\widetilde{\psi}_2(b,p)$ are also known, we have

$$\frac{1}{N_c^2-1} \sum_b \left[\frac{1}{\lambda_1} |\widetilde{\psi}_1(b,p)|^2 \,+\, \frac{1}{\lambda_2} |\widetilde{\psi}_2(b,p)|^2 \right] \,\leq\, G(p) \tag{10}$$

and

$$G(p) \,\leq\, \frac{1}{N_c^2-1} \sum_b \left[\frac{1}{\lambda_1} |\widetilde{\psi}_1(b,p)|^2 \,+\, \frac{1}{\lambda_2} \sum_{i:\lambda_i\neq 0,\lambda_1} |\widetilde{\psi}_i(b,p)\,|^2 \right] \;. \tag{11}$$

---

[4] Note that, at finite volume, the spectrum is discrete. For simplicity, we assume that the nonzero eigenvalues are non-degenerate. This is usually the case for nontrivial gauge configurations $A \neq 0$.

[5] Clearly, due to the relations (5), all the inequalities considered in this section usually hold strictly. However, we write all of them as non-strict inequalities, since we are mainly interested in estimates for the lower and upper bounds of the ghost propagator.

After adding and subtracting the quantity

$$\frac{1}{N_c^2-1}\,\frac{1}{\lambda_2}\,\sum_b \sum_{j:\lambda_j=0,\lambda_1} |\widetilde{\psi}_j(b,p)\,|^2 \tag{12}$$

and using again the completeness relation (8), the above upper bound can also be written as

$$G(p) \,\leq\, \frac{1}{N_c^2-1}\,\sum_b \left\{ \frac{1}{\lambda_1}\,|\widetilde{\psi}_1(b,p)|^2 \,+\, \frac{1}{\lambda_2}\left[1 - |\widetilde{\psi}_1(b,p)|^2 \,-\, \sum_{j:\lambda_j=0} |\widetilde{\psi}_j(b,p)\,|^2\right]\right\} \tag{13}$$

and, for nonzero momenta p, we are left with

$$\begin{aligned} G(p) &\leq \frac{1}{N_c^2-1}\,\sum_b \left\{ \frac{1}{\lambda_1}\,|\widetilde{\psi}_1(b,p)|^2 \,+\, \frac{1}{\lambda_2}\,\left[1 \,-\, |\widetilde{\psi}_1(b,p)|^2\right]\right\} \\ &= \left(\frac{1}{\lambda_1}-\frac{1}{\lambda_2}\right)\left(\frac{1}{N_c^2-1}\,\sum_b |\widetilde{\psi}_1(b,p)|^2\right) \,+\, \frac{1}{\lambda_2}\,. \end{aligned} \tag{14}$$

One can easily check that the new upper bound (14) is in general an improved bound compared to the original one [see Eq. (2) above]. Indeed, since the FP matrix is obtained from a second-order expansion, it can always be written in a symmetric form and its eigenvectors $\psi_i(b,x)$ can be assumed to be orthogonal to each other and normalized as $\sum_{b,x}\,|\psi_i(b,x)|^2 = 1$. Then, we have that[6]

$$\frac{1}{N_c^2-1}\,\sum_b\,|\widetilde{\psi}_1(b,p)|^2 \leq 1 \tag{15}$$

and the r.h.s. of the inequality (14) becomes

$$\left(\frac{1}{\lambda_1}-\frac{1}{\lambda_2}\right)\left(\frac{1}{N_c^2-1}\,\sum_b\,|\widetilde{\psi}_1(b,p)|^2\right) + \frac{1}{\lambda_2} \leq \frac{1}{N_c^2-1}\,\sum_b \left\{\left[\frac{1}{\lambda_1}-\frac{1}{\lambda_2}\right] + \frac{1}{\lambda_2}\right\} \,=\, \frac{1}{\lambda_1}\,. \tag{16}$$

For intermediate values of the lattice size N, one expects $\lambda_1 < \lambda_2$ and, at the same time, the upper bound (14) should be (numerically) strictly smaller than the previous upper bound $1/\lambda_1$. On the other hand, in the infinite-volume limit the spectrum of the FP matrix becomes continuous.[7] Thus, for very large values of N, the two smallest eigenvalues λ_1 and λ_2 should be almost equal, i.e. $\lambda_1 \lesssim \lambda_2$, and the two upper bounds will also be (almost) numerically equivalent. Therefore, the main conclusion of Ref. [36] is not modified: if λ_1 behaves as $N^{-2-\alpha}$ in the infinite-volume limit, we have that $\alpha > 0$ is a necessary condition to obtain a ghost propagator $G(p)$ enhanced in the infrared region (compared to the tree-level behavior $1/p^2$). Note that the bounds discussed here are valid for all momenta p, but we will generally be interested in the behavior of $G(p)$ for the smallest nonzero momentum p_{min}.

III. BOUNDS FOR $G(p_{min})$: NUMERICAL RESULTS

In this section we present data for the volume dependence of the ghost propagator at the smallest nonzero momentum $G(p_{min})$ and of the lower and upper bounds presented in the previous section [see Eqs. (2), (10) and (14)]. We also consider the dependence on the lattice volume V for the quantities entering the formulae of the bounds, i.e. the two smallest nonzero eigenvalues λ_1, λ_2 and the (average) projections

$$\overline{\psi}_s(p_{min}) \equiv \frac{1}{N_c^2-1}\,\sum_b\,\frac{1}{d}\,\sum_\mu\,\frac{1}{V}\,\left|\sum_x \psi_s(b,x)\,e^{-2\pi i x_\mu/N}\right|^2 \tag{17}$$

$$= \frac{1}{N_c^2-1}\,\sum_b\,\frac{1}{d}\,\sum_\mu\,\left|\widetilde{\psi}_s\left(b,\frac{2\pi}{N}\,e_\mu\right)\right|^2 \qquad s=1,2 \tag{18}$$

---

[6] Using the normalization condition for the eigenvalues $\psi_i(b,x)$ and considering the plane-wave functions $\phi_p(b,x) = \delta^{bc}\exp\left(2\pi i k\cdot x\right)/\sqrt{V}$, with $c = 1,2,\ldots,N_c^2-1$, the inequality (15) is just a consequence of the Cauchy-Schwarz-Bunyakovsky inequality and of the relation $\sum_{b,x}\,|\phi_p(b,x)|^2 = N_c^2-1$.

[7] For a numerical verification of this statement see, for example, Ref. [39] (Coulomb gauge) and Ref. [10] (Landau gauge).

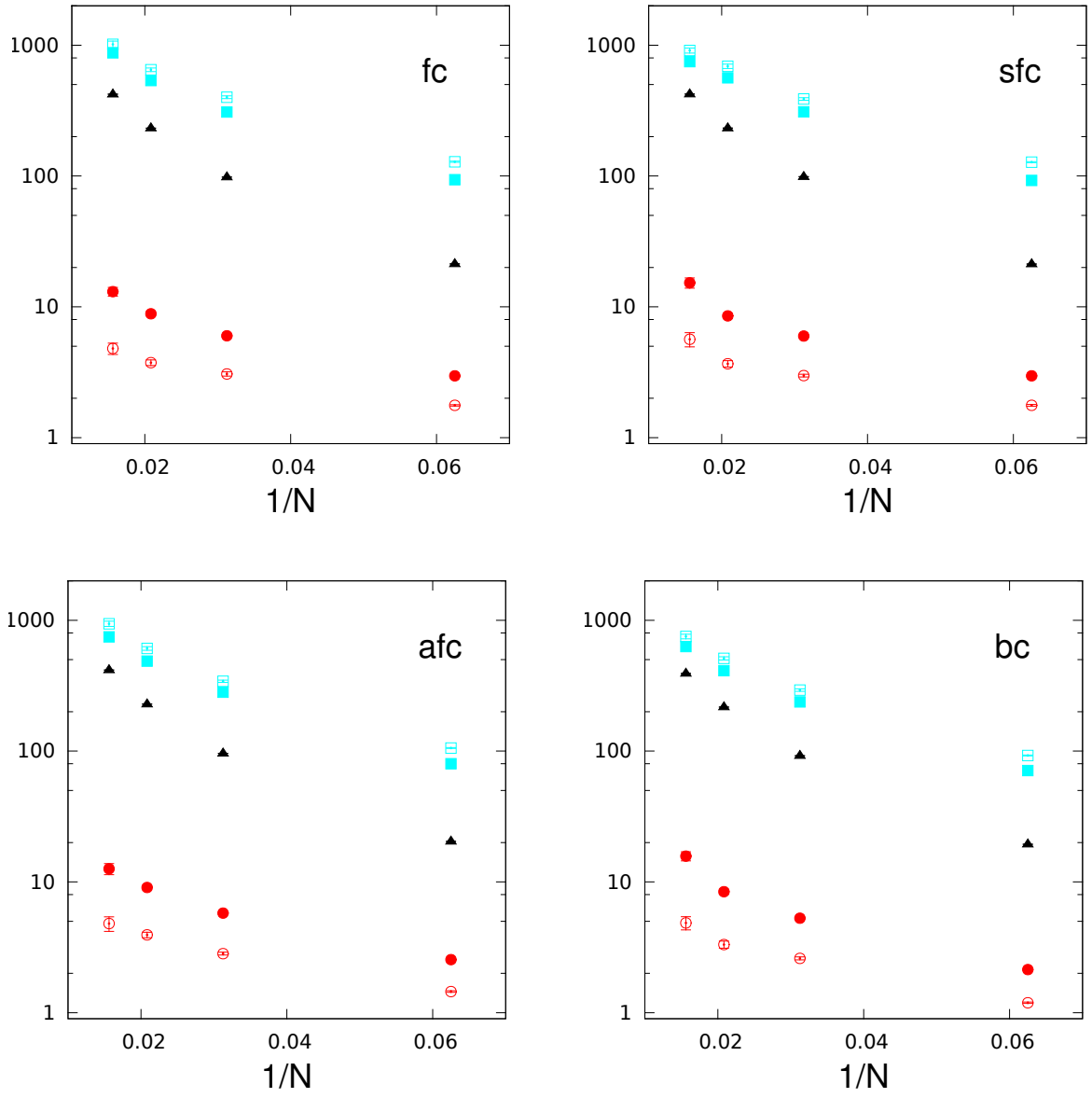


FIG. 1. The ghost propagator $G(p_{min})$ (full triangles), the lower bounds in Eqs. (2) and (10) (respectively empty and full circles) and the upper bounds in Eqs. (2) and (14) (respectively empty and full squares) as a function of the inverse lattice size $1/N$. All quantities are in lattice units. Four types of gauge-fixing prescription are considered (see Section III): *fc* (upper left plot), *sfc* (upper right plot), *afc* (lower left plot) and *bc* (lower right plot). Note the logarithmic scale on the y axis. The data points represent averages over gauge configurations, error bars correspond to one standard deviation. (We consider the statistical error only.)

of the eigenvectors $\psi_1(b,x)$ and $\psi_2(b,x)$ on the plane waves, which are d-fold degenerate and correspond to the smallest nonzero lattice momentum $p_{min} = 2\sin(\pi/N)$. The data have been generated using lattice numerical simulations for the SU(2) gauge group at $\beta = 2.2$, corresponding (see for example [40]) to a lattice spacing a of about 0.21 fm ≈ 1.066 GeV^{-1}. As discussed in Ref. [40], this value of β is in the scaling region. We considered lattice sizes $N = 16, 32, 48$ and 64 in the four-dimensional case[8] and four types of prescriptions for the numerical implementation of the minimal

[8] A total of 1600, 200, 100 and 50 thermalized configurations were, respectively, generated for these four lattice sizes.

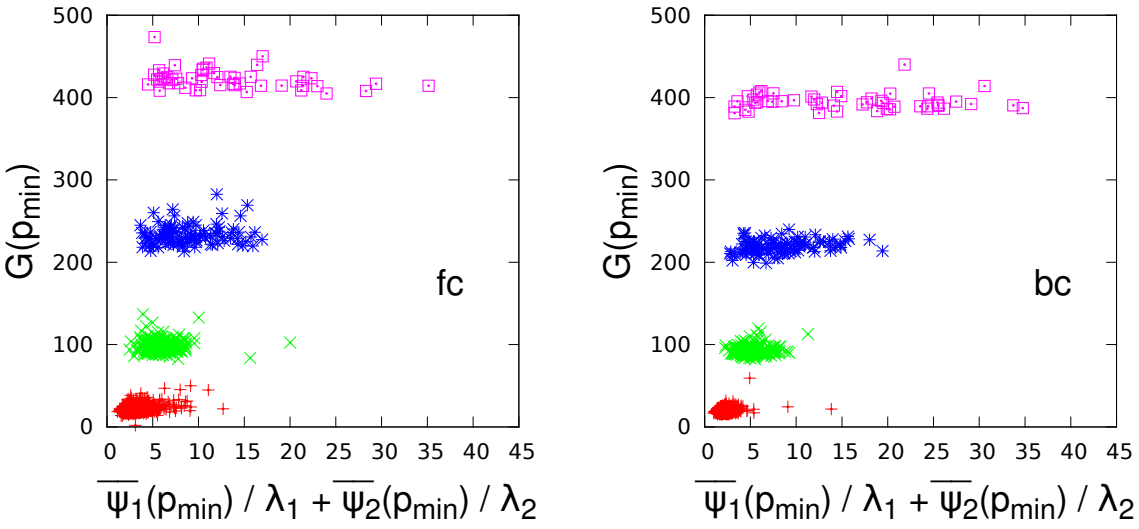


FIG. 2. The ghost propagator $G(p_{min})$ vs. the contribution to its value from the two smallest nonzero eigenvalues of the FP matrix [first two terms in Eq. (4)] for the lattice volumes $V = 16^4$ (red +), 32^4 (green $\times$), 48^4 (blue $*$) and 64^4 (magenta $\Box$) and for all the configurations used in our analysis. The quantities are in lattice units. Two types of Gribov copies are considered (see Section III): *fc* (left plot) and *bc* (right plot). Similar results have been obtained for the sets of Gribov copies indicated with *sfc* and *afc*.

Landau gauge.[9] More specifically, for each thermalized lattice configuration we fixed the gauge by using:

- a stochastic overrelaxation algorithm [41, 42] to obtain the first Gribov copy; we indicate this set of data below as first copy (*fc*);
- a smeared preconditioning [43], followed by a standard extremization (again using the stochastic overrelaxation algorithm), to obtain the first Gribov copy; we will refer to this set of data as smeared first copy (*sfc*);
- a stochastic-overrelaxed simulated annealing [44] — again to obtain the first Gribov copy — where we alternated one extremization sweep with five annealing steps;[10] this set of data will be called annealed first copy (*afc*);
- the same overrelaxed simulated annealing described in the above item but, this time, we considered for each configuration 16 Gribov copies, obtained by applying non-periodic Z(2) gauge transformations [24, 25]; among these copies we selected the one corresponding to the smallest value of the Landau-gauge minimizing functional; this set is indicated as best copy (*bc*).

The ghost propagator has been evaluated using a plane-wave source [17] and a point source [45], employing a conjugate-gradient method (with even/odd preconditioning) for the inversion of the FP matrix M. We have checked that the results obtained with these two methods are in agreement within the statistical error. As for the two smallest nonzero eigenvalues (and the corresponding eigenvectors) of M, they have been evaluated using the so-called power iteration method (see for example [46]). To this end, one needs to project out the subspace of constant eigenvectors, when evaluating λ_1, and the subspace spanned by constant eigenvectors and by ψ_1, when evaluating λ_2. The same eigenvalues have also been computed using a conjugate-gradient minimization of the so-called Ritz functional (or

[9] For the gauge field and for the minimizing functional defining the minimal Landau gauge, we consider the usual (unimproved) lattice definitions (see for example Ref. [3]).

[10] The complete annealing schedule consisted of 12500 steps with an increase of the inverse temperature by a factor of about 1.0007371 at each step.

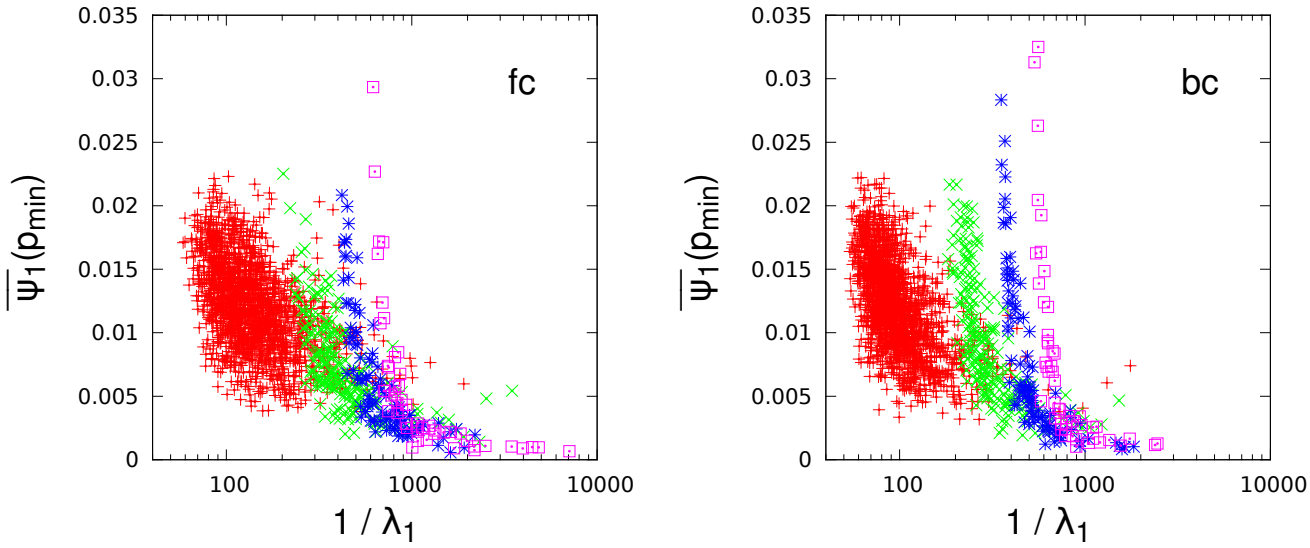


FIG. 3. Plot of the average projection $\overline{\psi}_1(p_{min})$ vs. the inverse of the smallest nonzero eigenvalue λ_1 for the lattice volumes $V = 16^4$ (red +), 32^4 (green $\times$), 48^4 (blue $*$) and 64^4 (magenta $\Box$) and for all the configurations used in our analysis. The quantities are in lattice units. Two types of Gribov copies are considered (see Section III): *fc* (left plot) and *bc* (right plot). Similar results have been obtained for the sets of Gribov copies indicated with *sfc* and *afc*. Note the logarithmic scale on the x axis.

Rayleigh quotient)

$$\zeta(\psi) \;=\; \frac{(\psi, \mathcal{M}\,\psi)}{(\psi,\, \psi)}\;, \tag{19}$$

based on the algorithm presented in Ref. [47]. Also in this case we checked that the different methods give results in agreement within their numerical accuracy.

Results for the ghost propagator $G(p)$, evaluated at the smallest nonzero momentum p_{min} using a plane-wave source, and for the two lower and the two upper bounds as a function of the inverse lattice size $1/N$ are reported in Figure 1, for the four types of gauge-fixing prescription described above. We see that, as the lattice size N increases, the value of $G(p_{min})$ gets closer to the two upper bounds. This result is in agreement with the data presented in Ref. [36] and suggests that, in the infinite-volume limit, one should find $G(p_{min}) \approx 1/\lambda_1$. At the same time, $G(p_{min})$ is much larger than the two lower bounds (and this difference seems to increase with the volume). This confirms the results presented in Ref. [10], where it was shown that one usually needs to consider the first 150–200 terms of Eq. (4) in order to reproduce the value of $G(p_{min})$ within a few percent. This observation is supported by the plots presented in Figure 2. From them one can also see that the relative spread of the contributions coming from the first two terms of Eq. (4) is much larger than the relative spread of the $G(p_{min})$ values, i.e. it is indeed the sum of several (correlated) terms in Eq. (4) that fixes the average value of $G(p_{min})$. Moreover, from Figures 3 and 4, it seems that, for large lattice volumes, this large spread gets complementary contributions from the projections $\overline{\psi}_s(p_{min})$ and from the factors $1/\lambda_s$. Indeed, for $N = 64$ and for $s = 1$ or 2, we can roughly divide the configurations in two sets: those characterized by a small, almost constant, value of $1/\lambda_s$ and by a large range of values for $\overline{\psi}_s(p_{min})$ and those characterized by a small, almost constant, value of $\overline{\psi}_s(p_{min})$ and by a large range of values for $1/\lambda_s$. As a consequence, the quantity $\overline{\psi}_s(p_{min})/\lambda_s$ shows a considerable spread, as can be seen in Figure 5 (see also Figure 2). At the same time, it is interesting to note that the spread and the distribution of the points for $\overline{\psi}_s(p_{min})/\lambda_s$, with $s = 1, 2$, are very similar for our largest lattice volume (see again Figure 5). This suggests that the two lowest eigenstates give a

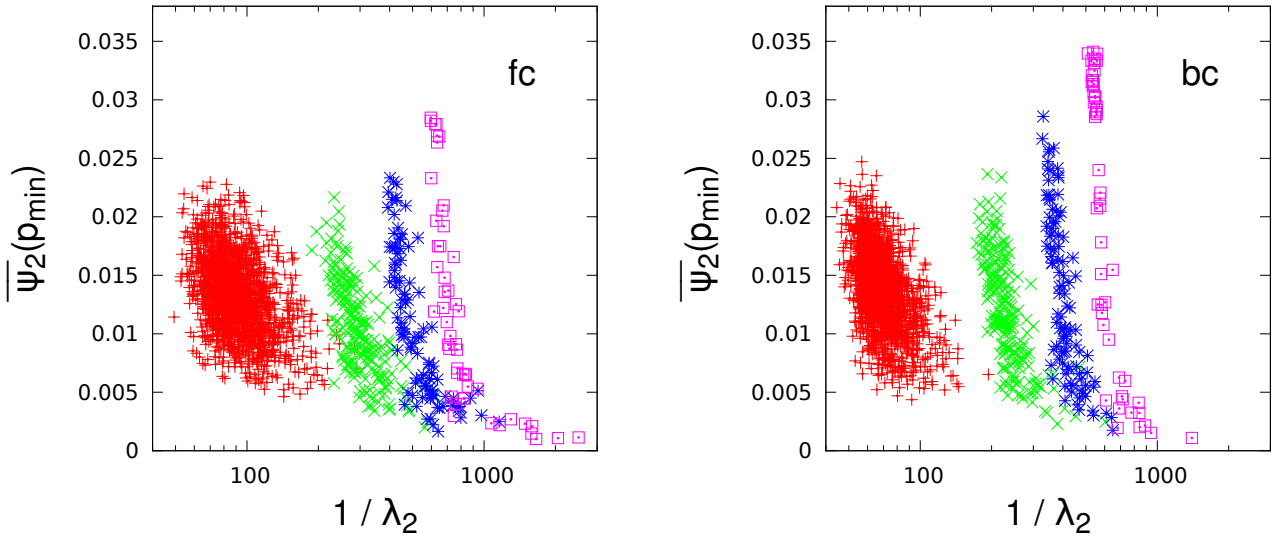


FIG. 4. Plot of the average projection $\overline{\psi}_2(p_{min})$ vs. the inverse of the second smallest nonzero eigenvalue λ_2 for the lattice volumes $V = 16^4$ (red +), 32^4 (green $\times$), 48^4 (blue $*$) and 64^4 (magenta $\square$) and for all the configurations used in our analysis. Two types of Gribov copies are considered (see Section III): *fc* (left plot) and *bc* (right plot). Similar results have been obtained for the sets of Gribov copies indicated with *sfc* and *afc*. Note the logarithmic scale on the x axis.

similar contribution to the ghost propagator for increasing volume,[11] as also discussed in the next paragraph.

In Figure 6 we show the statistical averages of λ_1 (full circles), λ_2 (empty circles), $\overline{\psi}_1(p_{min})$ (full squares) and $\overline{\psi}_2(p_{min})$ (empty squares) [see Eq. (18)] as a function of the inverse lattice size $1/N$. As discussed at the end of Section II, for very large lattice sizes one expects $\lambda_1 \lesssim \lambda_2$. Our data indeed suggest that, in the infinite-volume limit, these two eigenvalues become close to each other, in agreement with Ref. [10] (see their Figure 3). A nice visualization of this result is also presented in Figure 7 (note the log scale along both axes). As for the average projections $\overline{\psi}_s(p_{min})$, shown in Figure 6, we see that $\overline{\psi}_2(p_{min})$ has a minimum for N around 32 or 48 (which correspond to the two middle data points) and a larger value for $N = 64$ (which corresponds to the leftmost data point). The value of $\overline{\psi}_1(p_{min})$ seems strongly correlated with that of $\overline{\psi}_2(p_{min})$. On the other hand, its qualitative behavior is not the same for the four sets of data considered in our analysis. Indeed, in the limit of large N, when considering the prescriptions *fc* and *afc* we see for $\overline{\psi}_1(p_{min})$ a decreasing behavior (at a lower rate than for the eigenvalues), while for the choices *sfc* and *bc* the data suggest a plateau value of the order of 7×10^{-3}. Thus, in order to make a more conclusive analysis, it is probably necessary to simulate at larger lattice sizes[12]. At the same time, with only four data points it is not possible to carry out reliable tests of different fitting functions for the quantities considered in this work. For these reasons, we plan to extend, in the near future, the numerical simulations presented here.[13]

Finally, we note that the eigenvalues λ_1 and λ_2 (see Figures 6, 7 and the top plot in Figure 8) are clearly larger for the set of data *bc* — which can be viewed as a numerical attempt of constraining the functional integration to the fundamental modular region Λ — when compared to the other three sets of data. This is in agreement with the results presented in Refs. [10, 18]. Accordingly, the upper and lower bounds (see plots in Figure 1) are always smaller for the *bc* data than for the other sets. The same observation holds for the value of $G(p_{min})$, which is smaller for the *bc* set of data (see bottom plot in Figure 8), in agreement with Refs. [17, 19, 21–24, 26, 27]. Note that throughout

[11] One should stress that the eigenvectors ψ_1 and ψ_2 are always orthogonal when $\lambda_1 \neq \lambda_2$.

[12] Let us note that the lattice size $N = 64$ at $\beta = 2.2$ corresponds essentially to infinite volume regarding the study of the gluon propagator [48]. Nevertheless, different quantities usually display different finite-size effects. Moreover, also in the case of the gluon propagator, simulations up to $V = 128^4$ at $\beta = 2.2$ were necessary in order to achieve a clear description of its infrared behavior (see for example Ref. [49]).

[13] One should also stress that, due to the strong correlation among the data of $\overline{\psi}_1(p_{min})$ and $\overline{\psi}_2(p_{min})$, any quantitative study of their contribution to the ghost propagator in the infinite-volume limit would also require a full covariance analysis.

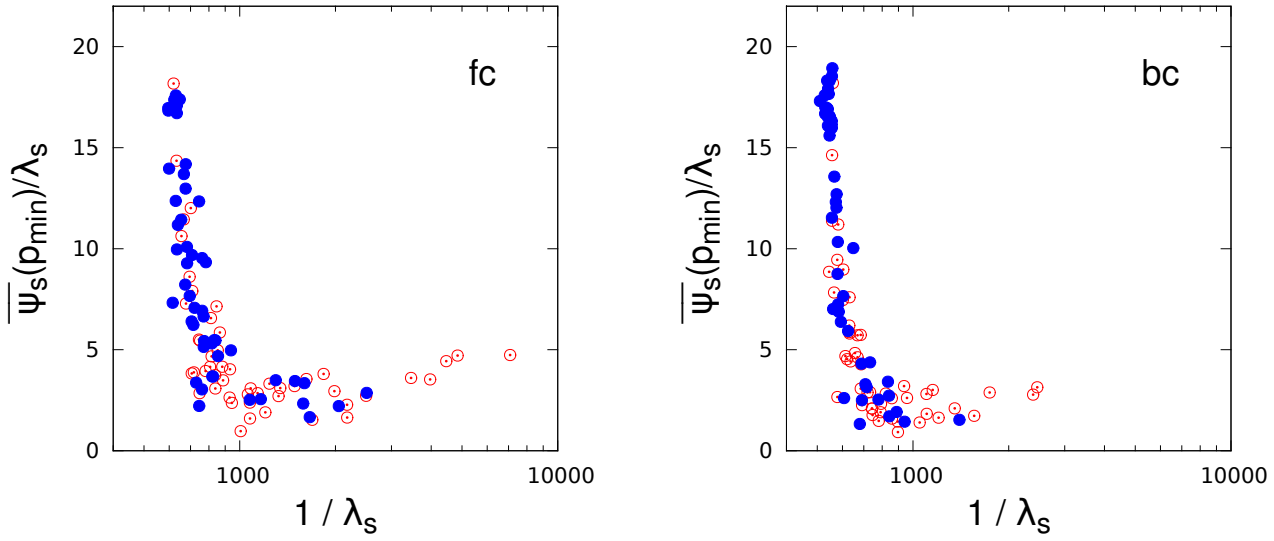


FIG. 5. Plot of the average projections $\overline{\psi}_s(p_{min})/\lambda_s$ vs. the inverse eigenvalue $1/\lambda_s$ for the lattice volume $V = 64^4$ and $s = 1$ (empty circles) or $s = 2$ (full circles), for all the configurations used in our analysis. The quantities are in lattice units. Two types of Gribov copies are considered (see Section III): *fc* (left plot) and *bc* (right plot). Similar results have been obtained for the sets of Gribov copies indicated with *sfc* and *afc*. Note the logarithmic scale on the x axis.

this section we have avoided direct comparisons of our data for the four different averages in the same plot. In fact, we found that such plots were, in general, difficult to visualize. In Figure 8, for example, the data corresponding to the remaining two types of averages lie somewhere between the two cases displayed.

IV. LOWER BOUND FOR λ_1

In Section II we recalled our proof of the lower and upper bounds for the ghost propagator $G(p)$ — written in terms of the smallest nonzero eigenvalue λ_1 (and of the corresponding eigenvector) of the FP matrix [36] — and showed how these bounds can be improved, for example by considering the two smallest nonzero eigenvalues λ_1 and λ_2 (and the corresponding eigenvectors). In Section III these results were compared to data obtained in four-dimensional numerical simulations of the SU(2) case in minimal Landau gauge, considering different sets of local minima. In this section we present a simple lower bound for λ_1, which constrains its approach to zero in the infinite-volume limit. This result will be numerically verified in the next section. This new bound will also help us get a better understanding of the infinite-volume limit in minimal Landau gauge, which in turn is discussed in Section VI.

Our proof is based on the concavity of the minimum function (see for example Section 12.4 in [50]) and on three important properties of the first Gribov region Ω in Landau gauge (see for example Section 2.1.3 in [6], Section 2.2.1 in [7], Appendix C in Ref. [31] and Ref. [51]):

1. the trivial vacuum $A_\mu = 0$ belongs to Ω;
2. the region Ω is convex;
3. the region Ω is bounded in every direction.

These three properties[14] can be proved by recalling that the region Ω is defined as the set of gauge configurations A_μ

[14] One should also recall that all gauge orbits intersect the first Gribov region [52].

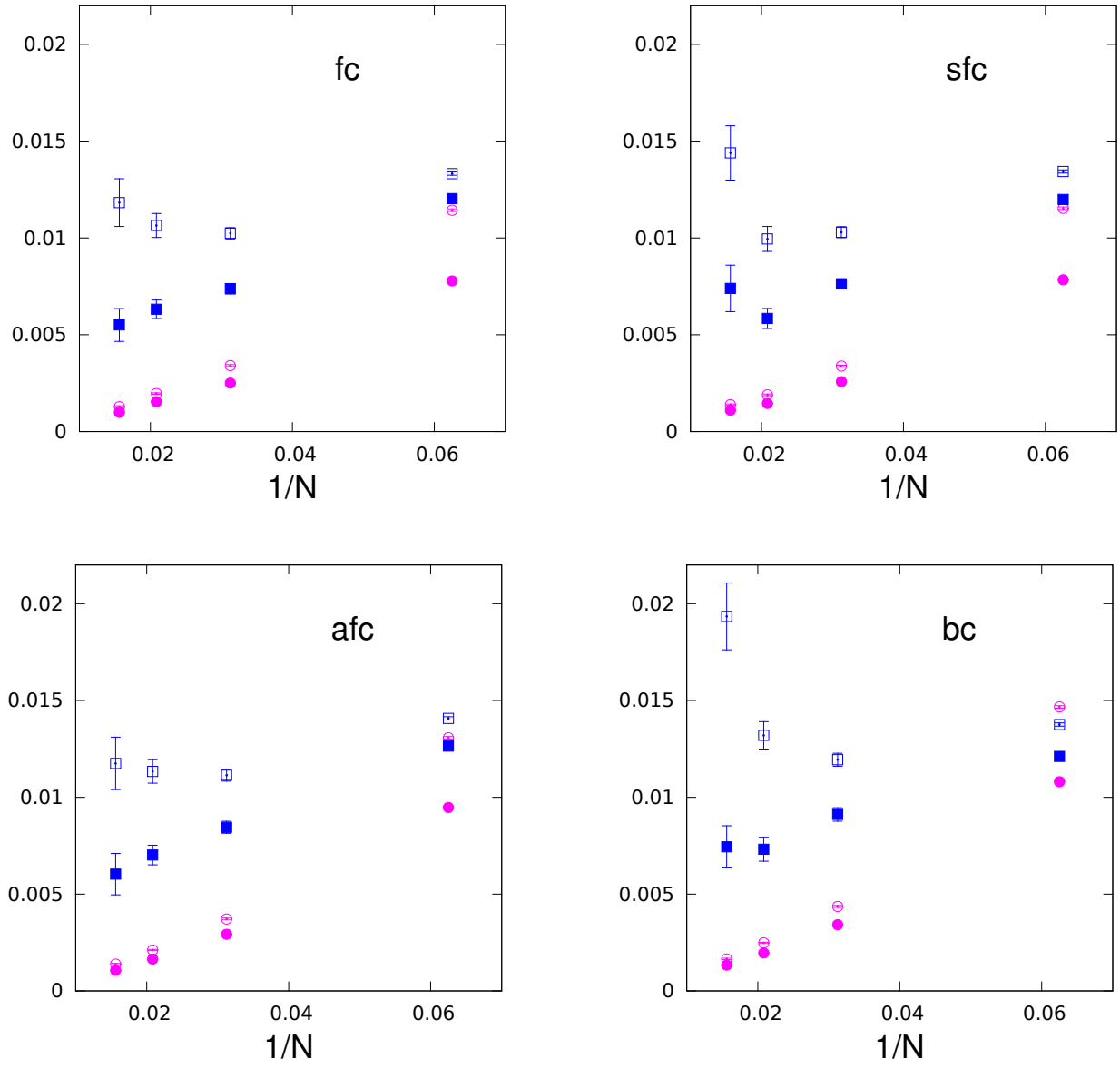


FIG. 6. The two smallest nonzero eigenvalues λ_1 (full circles) and λ_2 (empty circles) and the two average projections $\overline{\psi}_1(p_{min})$ (full squares) and $\overline{\psi}_2(p_{min})$ (empty squares) [see Eq. (18)], as a function of the inverse lattice size $1/N$. All quantities are in lattice units. Four types of gauge-fixing prescription are considered (see Section III): *fc* (upper left plot), *sfc* (upper right plot), *afc* (lower left plot) and *bc* (lower right plot). The data points represent averages over gauge configurations, error bars correspond to one standard deviation. (We consider the statistical error only.)

that are transverse, i.e. $\partial \cdot A = 0$, and for which the FP operator

$$\mathcal{M}(b,x;c,y)[A] \;=\; -\partial \cdot D^{bc}(x,y)[A] \tag{20}$$

is semi-positive definite. Here, $D^{bc}(x,y)[A]$ is the covariant derivative. Then, the first property follows immediately, nothing that a null value for A_μ implies $\mathcal{M}(b,x;c,y)[0]$ equal to (minus) the Laplacian, which is a semi-positive definite operator.

Concerning the second property listed above, the key ingredient of the proof is that the gauge condition $\partial \cdot A = 0$ and the operator $D^{bc}(x,y)[A]$ — and therefore also the FP operator $\mathcal{M}(b,x;c,y)[A]$ — are linear in the gauge field

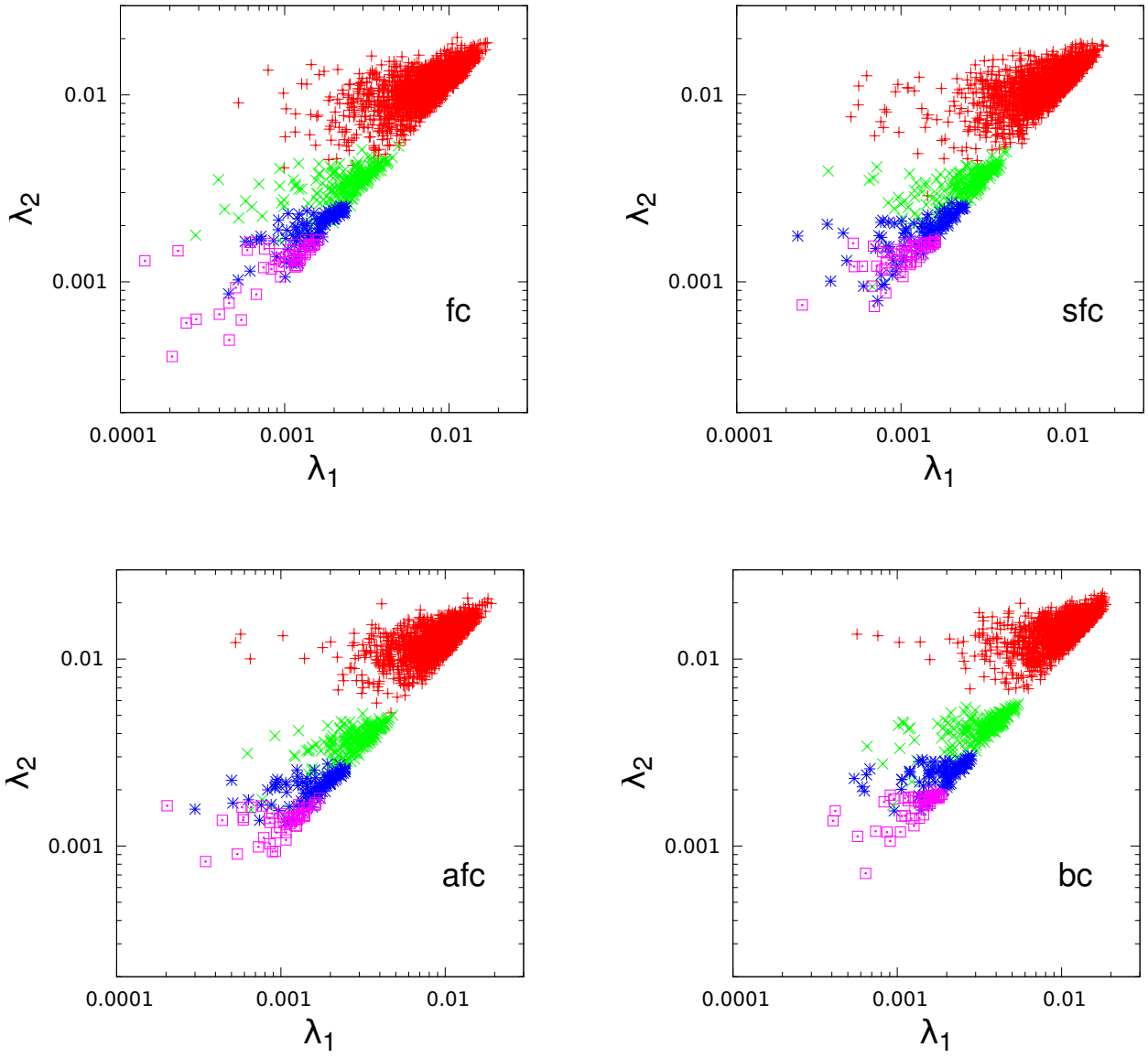


FIG. 7. Plot of the second smallest nonzero eigenvalue λ_2 vs. the smallest nonzero eigenvalue λ_1 for the lattice volumes $V = 16^4$ (red +), 32^4 (green $\times$), 48^4 (blue $*$) and 64^4 (magenta $\Box$) and for all the configurations used in our analysis. The quantities are in lattice units. Four types of Gribov copies are considered (see Section III): *fc* (upper left plot), *sfc* (upper right plot), *afc* (lower left plot) and *bc* (lower right plot). Note the logarithmic scale on both axes.

A_μ. Indeed, if we write[15]

$$\mathcal{M}[A] \;=\; -\partial^2 + \mathcal{K}[A] \tag{21}$$

and we consider the linearity of the operator $\mathcal{K}[A] \sim [A_\mu, \partial_\mu]$, we find that

$$\mathcal{M}[(1-\rho)A_1 + \rho A_2] = -\partial^2 + \mathcal{K}[(1-\rho)A_1 + \rho A_2] \;=\; -\partial^2 + (1-\rho)\mathcal{K}[A_1] + \rho\,\mathcal{K}[A_2]$$

[15] Here and below we simplify the notation and, unless necessary, we do not explicitly show the color and space-time indices of the operators.

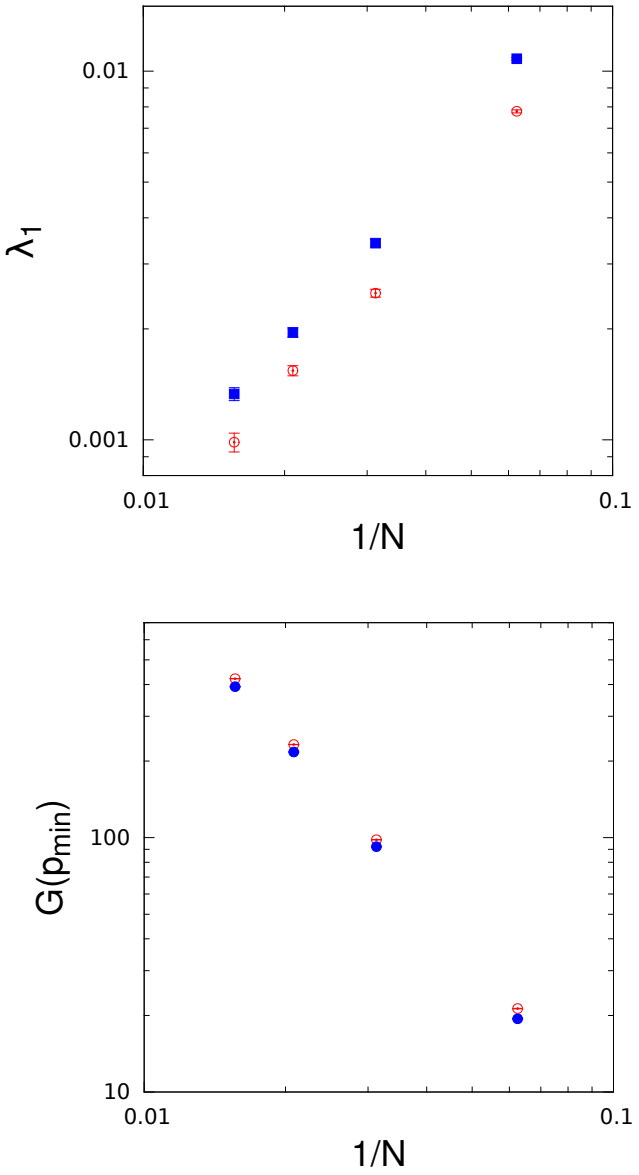


FIG. 8. The smallest nonzero eigenvalue λ_1 (top plot) and the ghost propagator $G(p_{min})$ evaluated at the smallest nonzero momentum p_{min} (bottom plot) for the *fc* data (empty circles) and for the *bc* data (full circles), as a function of the inverse lattice size $1/N$. All quantities are in lattice units. Note the logarithmic scale on both axes. The data points represent averages over gauge configurations, error bars correspond to one standard deviation. (We consider the statistical error only.)

$$= (1-\rho)\left(-\partial^2 + \mathcal{K}[A_1]\right) + \rho\left(-\partial^2 + \mathcal{K}[A_2]\right) \tag{22}$$

$$= (1-\rho)\mathcal{M}[A_1] + \rho\,\mathcal{M}[A_2]\,. \tag{23}$$

Then, for $\rho \in [0,1]$, it is clear that $\mathcal{M}[(1-\rho)A_1 + \rho A_2]$ is semi-positive definite if $\mathcal{M}[A_1]$ and $\mathcal{M}[A_2]$ are also semi-positive definite. At the same time, we have

$$(1-\rho)\,\partial\cdot A_1 + \rho\,\partial\cdot A_2 = 0 \tag{24}$$

if $\partial\cdot A_1 = \partial\cdot A_2 = 0$. Thus, the convex combination $(1-\rho)A_1 + \rho A_2$ belongs to Ω, for any value of $\rho \in [0,1]$, if $A_1, A_2 \in \Omega$. This proves the second property of Ω. By combining properties 1 and 2, we can now set $A_1 = 0$, $A_2 = A$

and consider the configuration ρA. In this case Eq. (22) becomes

$$\mathcal{M}[\rho A] = -\partial^2 + \mathcal{K}[\rho A] \;=\; (1-\rho)\,(-\partial^2) \;+\; \rho\,\big(-\partial^2 + \mathcal{K}[A]\big) \tag{25}$$

$$= (1-\rho)\,(-\partial^2) \;+\; \rho\,\mathcal{M}[A] \tag{26}$$

and, if A belongs to Ω, we have already proven that ρA is also an element of Ω for any value of $\rho \in [0,1]$. On the other hand, we can show that, for a sufficiently large value of $\rho > 1$, the configuration ρA lies outside of the region Ω, i.e. the matrix

$$\mathcal{M}[\rho A] \;=\; -\partial^2 + \mathcal{K}[\rho A] \;=\; -\partial^2 + \rho\,\mathcal{K}[A] \tag{27}$$

is not semi-positive definite. In this case the important observation is that the trace of the operator $\mathcal{K}[A]$ is zero. More specifically, since the color indices of $\mathcal{K}[A]$ are given by $\mathcal{K}^{bc}[A] \sim f^{bce} A^e_\mu$ [where f^{bce} are the structure constants of the SU(N_c) group] and since these structure constants are completely (color) anti-symmetric, we have that all the diagonal elements of $\mathcal{K}[A]$ are zero. This implies that the sum of the eigenvalues of $\mathcal{K}[A]$ is also zero. Moreover, the operator $\mathcal{K}[A]$ is real and symmetric (i.e. invariant under simultaneous interchange of x with y and b with c), implying that its eigenvalues are real. Thus, at least one of the eigenvalues of $\mathcal{K}[A]$ is (real and) negative. Then, if we indicate with ϕ_{neg} the corresponding eigenvector, it is clear that for a sufficiently large (but finite) value of $\rho > 1$ the scalar product $(\phi_{neg}, \mathcal{M}[\rho A]\phi_{neg})$ must be negative, so that $\mathcal{M}[\rho A]$ is not semi-positive definite and the configuration ρA does not belong to Ω.

Using Eq. (26) above we can now find a lower bound for the smallest nonzero eigenvalue. To this end we consider a configuration A' belonging to the boundary $\partial\Omega$ of Ω and we write[16]

$$\lambda_1\left[\,\mathcal{M}[\rho A']\,\right] \;=\; \lambda_1\left[(1-\rho)\,(-\partial^2) \;+\; \rho\,\mathcal{M}[A']\right] \tag{28}$$

for $\rho \in \Re$. From the second property of Ω we know that $\rho A' \in \Omega$ for $\rho \in [0,1]$. At the same time, we have

$$\lambda_1\left[(1-\rho)\,(-\partial^2) \;+\; \rho\,\mathcal{M}[A']\right] \;=\; \min_{\chi \neq \text{constant}} \left(\chi\,,\left[\,(1-\rho)\,(-\partial^2) \;+\; \rho\,\mathcal{M}[A']\,\right]\,\chi\right)\;, \tag{29}$$

where the vectors $\chi(b,x)$ are assumed to be normalized as $(\chi\,,\chi) = 1$. Then, using the concavity of the minimum function [50] we obtain

$$\lambda_1\left[\,\mathcal{M}[\rho A']\,\right] = \min_{\chi \neq \text{constant}} \left(\chi\,,\left[\,(1-\rho)\,(-\partial^2) \;+\; \rho\,\mathcal{M}[A']\,\right]\,\chi\right) \tag{30}$$

$$\geq (1-\rho) \min_{\chi \neq \text{constant}} \left(\chi\,,(-\partial^2)\,\chi\right) \;+\; \rho \min_{\chi \neq \text{constant}} \left(\chi\,,\mathcal{M}[A']\,\chi\right)$$

$$= (1-\rho)\,\lambda_1\left[\,-\partial^2\right] \;+\; \rho\,\lambda_1\left[\,\mathcal{M}[A']\,\right]$$

$$= (1-\rho)\,p^2_{min}\;, \tag{31}$$

where in the last step we used the fact that $A' \in \partial\Omega$, i.e. the smallest non-trivial eigenvalue of the FP matrix $\mathcal{M}[A']$ is null, and that the smallest non-trivial eigenvalue of (minus) the Laplacian $-\partial^2$ is the magnitude squared of the smallest nonzero momentum p^2_{min}. (Let us recall that this eigenvalue is d-fold degenerate.) Therefore, as the lattice size N goes to infinity, we find that $\lambda_1\left[\,\mathcal{M}[\rho A']\,\right]$ cannot go to zero faster than $(1-\rho)\,p^2_{min}$. At the same time, since p^2_{min} behaves as $1/N^2$ at large N, we have that λ_1 behaves as $N^{-2-\alpha}$ in the same limit, with $\alpha > 0$, only if the quantity $1-\rho$ goes to zero at least as fast as $N^{-\alpha}$. It is also interesting to note that in the Abelian case one has $\mathcal{M} = -\partial^2$ and therefore $\lambda_1 = p^2_{min}$. Thus, all the non-Abelian effects of the theory are essentially included in the $(1-\rho)$ factor.[17] It is furthermore important to stress that the above result applies to any Gribov copy belonging to

---

[16] Here and below, we indicate with $\lambda_1\,[\mathcal{M}]$ the smallest nonzero eigenvalue of the matrix $\mathcal{M}$.

[17] For a numerical verification of the inequality, see Section VI.

Ω. (Clearly, different Gribov copies $A^{(g)}$ will have different values of ρ.) Finally, note that the above inequality may equivalently be written as

$$\lambda_1 \left[\mathcal{M}[A] \right] \, \geq \, (1-\rho) \, p^2_{min} \, , \tag{32}$$

where $\rho \leq 1$ measures the distance of a generic configuration $A \in \Omega$ from the "origin" $A = 0$ (in such a way that $\rho^{-1} A$ will lie on $\partial\Omega$).

A fortuitous feature of the above bound is that it is written in terms of the smallest nonzero lattice momentum. Then, if we combine this lower bound for λ_1 with the upper bound in Eq. (2), we find

$$G(p) \, \leq \, \frac{1}{\lambda_1} \, \leq \, \frac{1}{[1-\rho] \, p^2_{min}} \, , \tag{33}$$

where we have stressed that all quantities have been evaluated for the gauge configuration A. Thus, in order to have a ghost propagator $G(p)$ enhanced in the infrared limit (compared to the tree-level behavior $1/p^2$), a necessary condition is that the quantity $1-\rho$ go to zero sufficiently fast in the infinite-volume limit. Moreover, for $p = p_{min}$ and by writing the ghost propagator as

$$G(p_{min}) \, = \, \frac{1}{p^2_{min}} \, \frac{1}{1-\sigma(p_{min})} \, , \tag{34}$$

where $\sigma(p)$ is the Gribov ghost form-factor, we have the inequality

$$\sigma(p_{min}) \, \leq \, \rho \tag{35}$$

[with $\rho \leq 1$]. Let us recall that the restriction of the physical configuration space to the region Ω is usually done by imposing the so-called no-pole condition (see for example [53, 54] and references therein)

$$\sigma(p) < 1 \qquad \text{for} \qquad p^2 > 0 \tag{36}$$

and that $\sigma(p)$ is monotonically decreasing as p^2 increases (see Section 2.D in Ref. [53]). Here we have proven that, for a given lattice configuration $A \in \Omega$, the Gribov ghost form-factor satisfies the stronger inequality (35), which is related to a simple geometrical characterization of the configuration A.

Another simple consequence of Eq. (33) is an upper bound for the so-called b parameter, used to characterize different Gribov copies in Refs. [28, 55]. Note that, on the lattice, the b factor is proportional to the ghost propagator $G(p)$ evaluated at the smallest nonzero momentum p_{min}. Thus, if we indicate this proportionality constant with ν^2, we can write

$$\max \, b[A] \, \leq \, \frac{\nu^2}{p^2_{min}} \, \max_g \frac{1}{1-\rho\left[A^{(g)}\right]} \, , \tag{37}$$

where the configurations $\{A\}$ and $\left\{A^{(g)}\right\}$ are related by the gauge transformation g and the maximum is taken over all Gribov copies in Ω. We see that the volume dependence of the upper bound for the b parameter is given by the approach to 1 of the quantity $\max_g \rho\left[A^{(g)}\right]$ towards the infinite-volume limit (and by how well the upper bound is saturated). This could explain the over-scaling observed in Ref. [29] using simulations at $\beta = 0$, apparently in violation of the uniqueness result [56] for the scaling solution [57–60] of the Dyson-Schwinger equations for gluon and ghost propagators. Indeed, in the strong-coupling regime, most Gribov copies should be just lattice artifacts not related to the continuum theory, such as the lattice configurations inducing confinement in the compact $U(1)$ case. Therefore, it is conceivable that an exhaustive search of Gribov copies might generate a gauge-fixed configuration $A^{(g)}$ characterized by a value of $\rho\left[A^{(g)}\right]$ very close to 1 and almost saturation of the bound (37). In this way, strong-coupling lattice artifacts would produce an overly enhanced ghost propagator in the infrared limit.

Finally, following the analysis in Section 3 of Ref. [4], we can consider (in a finite lattice volume) the nonzero eigenvalues $\overline{\lambda} = p^2(k)$ (for $k \neq 0$) of the operator $\mathcal{M}(b,x;c,y)[0] = -\delta^{bc} \, \delta^d(x-y) \, \partial^2$, which are characterized by

a degree of degeneracy $g(\overline{\lambda})$. [For example, for the smallest nonzero eigenvalue p^2_{min} one has $g(\overline{\lambda}) = d(N_c^2 - 1)$.] This degeneracy is in general lifted for the eigenvalues λ of the operator $\mathcal{M}(b, x; c, y)[A]$, where A is a generic gauge configuration. More precisely, to a given eigenvalue $\overline{\lambda}(p) = p^2$, with degeneracy g, one can associate the eigenvalues $\lambda_i(p)$ of $\mathcal{M}(b, x; c, y)[A]$, with $i = 1, 2, \ldots, g$ and $\lambda_i(0, p) = p^2$. By rescaling these eigenvalues by $\overline{\lambda}(p)$, i.e. by considering the ratios

$$L_i(p) \, = \, \frac{\lambda_i(p)}{p^2} \, , \tag{38}$$

and after defining the center of gravity

$$m(p) \, = \, \frac{1}{g} \, \sum_{i=1}^{g} \, L_i(p) \, , \tag{39}$$

it was proven in Appendix C of Ref. [4] that, for very large volumes, the following equality holds

$$m(p) \, = \, 1 \, - \, \frac{H}{dV(N_c^2 - 1)} \, , \tag{40}$$

where H is the so-called horizon function, defined in Eq. (3.10) of [4]. Since the r.h.s. of the above result is independent of the momentum p, we can evaluate it at the smallest nonzero eigenvalue $\overline{\lambda} = p^2_{min}$ of $\mathcal{M}(b, x; c, y)[0]$. At the same time we have that $\lambda_i(p_{min}) \geq \lambda_1$, where λ_1 is the smallest nonzero eigenvalue of $\mathcal{M}(b, x; c, y)[A]$, implying $L_i(p_{min}) \geq \lambda_1 / p^2_{min}$. As a consequence, using the inequality (32), we obtain

$$m(p_{min}) \, \geq \, \frac{\lambda_1}{p^2_{min}} \, \geq \, 1 \, - \, \rho \tag{41}$$

and the theorem in Eq. (40) yields

$$\frac{H}{dV(N_c^2 - 1)} \, \equiv \, h \, \leq \, \rho \, . \tag{42}$$

One immediately notices that this result is very similar to the bound in (35). This is not surprising since it has been recently proven [54] that, in the continuum and to all orders in the gauge coupling, the Gribov ghost form-factor $\sigma(0)$ at zero momentum is indeed equal to the normalized horizon function h.

We can conclude this section by stressing that our new bounds [see Eqs. (32), (33), (35) and (42)] suggest all non-perturbative features of a minimal-Landau-gauge configuration $A \in \Omega$ to be related to its normalized distance ρ from the "origin" $A = 0$ (or, equivalently, to its normalized distance $1 - \rho$ from the boundary $\partial\Omega$). The same formulae also represent a clear mathematical description[18] of the crucial role of the boundary $\partial\Omega$ in the Gribov-Zwanziger approach.

V. LOWER BOUND FOR λ_1: NUMERICAL RESULTS

One can verify numerically some of the analytic results presented in the previous section. In particular, one can check the third property of the region Ω, presented at the beginning of the section, and the new bound (32) — or, equivalently, the sequence of bounds in Eq. (33) — as well as the bounds (35) and (42). To this end, we have generated 70 new configurations for $V = 16^4, 24^4, 32^4$ and 40^4 at $\beta = 2.2$ and 50 new configurations for $V = 48^4, 56^4, 64^4, 72^4$ and 80^4 at the same β value. For each of these thermalized configurations[19] we have evaluated the ghost propagator $G(p)$, the two smallest nonzero eigenvalues and the respective eigenvectors. We then studied the geometrical properties

---

[18] One can compare, for example, the above result (42) to the qualitative discussion presented in the Conclusions of Ref. [5].

[19] For the gauge fixing we used a stochastic overrelaxation algorithm for the first Gribov copy, i.e. these data correspond to the statistical average of the gauge-fixing prescription indicated above with *fc*. Of course, the same numerical analysis can also be carried out for the other three types of statistical averages considered in Section III.

N	$\max(n)$	$\min(n)$	$\langle n \rangle$	$R_{\rm before}$	$R_{\rm after}$
16	30	6	17.2	15(3)	-30(12)
24	27	4	15.1	20(7)	-26(6)
32	19	5	11.7	26(9)	-51(20)
40	18	4	9.4	155(143)	-21(6)
48	13	2	7.8	21(5)	-21(5)
56	12	3	7.6	16(4)	-21(7)
64	11	2	6.8	20(7)	-42(18)
72	11	2	6.1	129(96)	-42(13)
80	12	3	6.1	15(4)	-24(4)

TABLE I. The maximum, minimum and average number of steps n, necessary to "cross the Gribov horizon" along the direction $A^b_\mu(x)$, as a function of the lattice size N. We also show the ratio R [see Eq. (43)], divided by 1000, for the modified gauge fields $\tau_{n-1} A^b_\mu(x)$ and $\tau_n A^b_\mu(x)$, i.e. for the configurations immediately before and after crossing $\partial\Omega$. Here we used the gauge-fixing prescription *fc* (see Section III). The data in the last two columns represent averages over gauge configurations, errors correspond to one standard deviation. (We consider the statistical error only.)

discussed in the previous section, by applying scale transformations[20] to the gauge configuration A. More precisely, we multiply the gauge-fixed gauge field $A_\mu(x)$ by a constant factor τ_1, slightly larger than 1. Clearly, the new gauge field $A^{(1)}_\mu(x) = \tau_1 A_\mu(x)$ still satisfies the Landau gauge condition $\partial_\mu A^{(1)}_\mu(x) = 0$. Also, if τ_1 is not too large, it can be verified that the smallest nonzero eigenvalue of $\mathcal{M}[A^{(1)}]$ remains positive, i.e. the configuration $A^{(1)}$ belongs to the first Gribov region Ω. By iterating this procedure, we consider a sequence of values τ_2, τ_3, ... for the scale transformation[21] of A. After n steps, we end up with a modified gauge field $A^{(n)}_\mu(x) = \tau_n A_\mu(x)$ that does not belong anymore to the region Ω, i.e. the eigenvalue λ_1 of $\mathcal{M}[A^{(n)}]$ is negative (while λ_2 is still positive). In Table I we report, for each lattice size N, the average number of steps $\langle n \rangle$ necessary to find a modified gauge field $\tau_n A_\mu(x) \notin \Omega$. We also show, for each N, the largest and the smallest values of n. This represents a direct verification of the third property described in the previous section. It is also interesting to note that the number of steps n necessary to "bring" the gauge configuration outside the region Ω decreases with N, confirming that configurations with larger physical volume are (on average) closer to the boundary $\partial\Omega$.

For each configuration we also show, in the same table, the average value of the ratio

$$R = \frac{(\,\mathcal{E}'''\,)^2}{\mathcal{E}''\;\mathcal{E}''''} \tag{43}$$

just before and just after crossing $\partial\Omega$. Here $\mathcal{E}''$, $\mathcal{E}'''$ and $\mathcal{E}''''$ are, respectively, the second, third and fourth derivatives of the minimizing functional $\mathcal{E}[A]$ [see Eq. (1)] evaluated along the direction defined by the eigenvector $\psi_1(b,x)$.[22] As shown in Ref. [18], this ratio characterizes the shape of the minimizing functional $\mathcal{E}$, around the local minimum considered, when one applies to $\mathcal{E}$ a fourth-order Taylor expansion (see in particular Figure 2 of the same reference). We find that this ratio is the only quantity that shows an abrupt jump across the boundary $\partial\Omega$ (see the top plot in Fig. 9). Indeed, we checked that the second, third and fourth derivatives, as well as the various terms contributing to them and defined in Eqs. (11), (13) and (14) of Ref. [18], have a slow and continuous dependence on the factors τ_i (see for example the bottom plot in Fig. 9 and in Fig. 10). On the other hand, since $\mathcal{E}''$ decreases as τ_i increases, we find that the ratio R usually increases with τ_i and that $R_{n-1} \approx -R_n$, due to the change in sign of $\mathcal{E}''$ as the first

[20] One should stress that this procedure is a simple way of "simulating" the mathematical proofs presented in the previous section. On the other hand, by rescaling the gauge field we withdraw the unitarity of the link variables, thus loosing the connection with the usual Monte Carlo simulations. Nevertheless, as it will be shown below, this approach gives us useful insights into the properties of the Faddeev-Popov matrix and of the first Gribov region.

[21] For the factor τ_i we used the following prescription: $\tau_0 = 1$, $\tau_i = \delta\,\tau_{i-1}$, $\delta = 1.001$ if $\lambda_1 \geq 5 \times 10^{-3}$, $\delta = 1.0005$ if $\lambda_1 \in [5 \times 10^{-4}, 5 \times 10^{-3})$ and $\delta = 1.0001$ if $\lambda_1 < 5 \times 10^{-4}$, with λ_1 evaluated at the step $i-1$.

[22] One should note that, then, $\mathcal{E}'' = \lambda_1$.

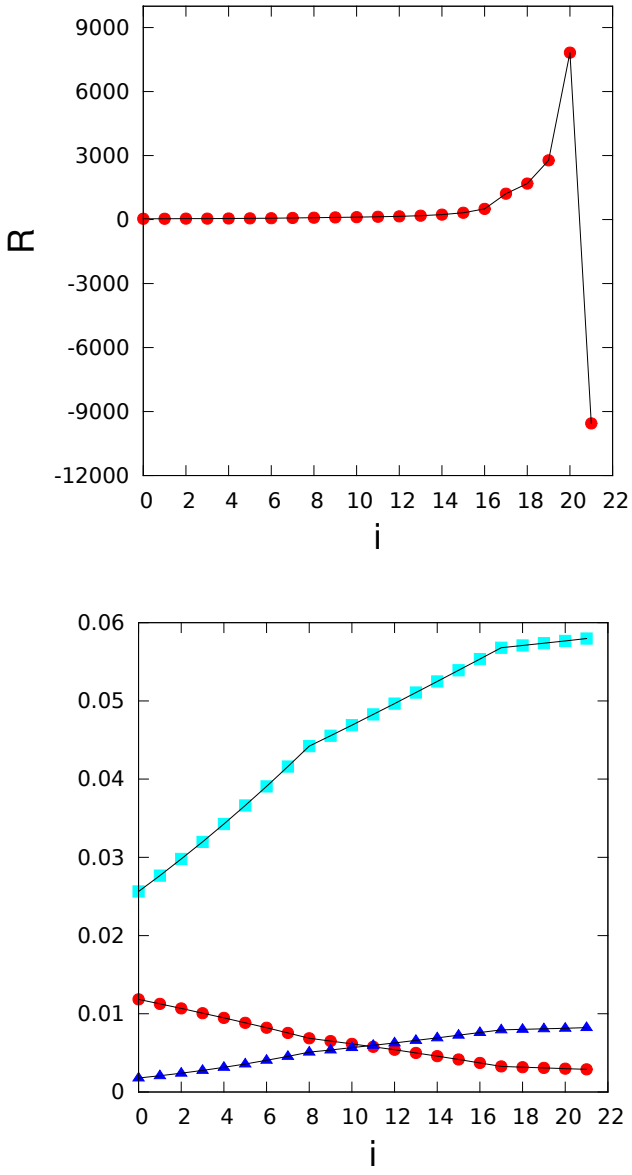


FIG. 9. Top plot: the ratio R [see Eq. (43)], as a function of the iteration step i, for a typical configuration with lattice volume 16^4. Bottom plot: the second smallest (non-trivial) eigenvalue λ_2 (full circles), the absolute value of the third derivative of the minimizing function $|\mathcal{E}'''|$ (full squares) and the fourth derivative of the minimizing function $\mathcal{E}''''$ (full triangles) as a function of the iteration step i, for the same configuration considered in the top plot. One can easily recognize the three different values for the δ step used in the iteration process (see footnote 21). Here we used the gauge-fixing prescription *fc* (see Section III). In all cases the solid line is only to guide the eye.

Gribov horizon is crossed (see the fourth and the fifth columns in Table I). This behavior can also be seen in the top plot of Figure 9, where the value of R is shown (as a function of the number of steps i) for one of the typical configurations generated for the volume 16^4. At the same time one can check (see the bottom plot in Figure 9) that the second smallest (non-trivial) eigenvalue stays positive, i.e. the final configuration $\tau_n A_\mu(x)$ belongs to the second Gribov region.

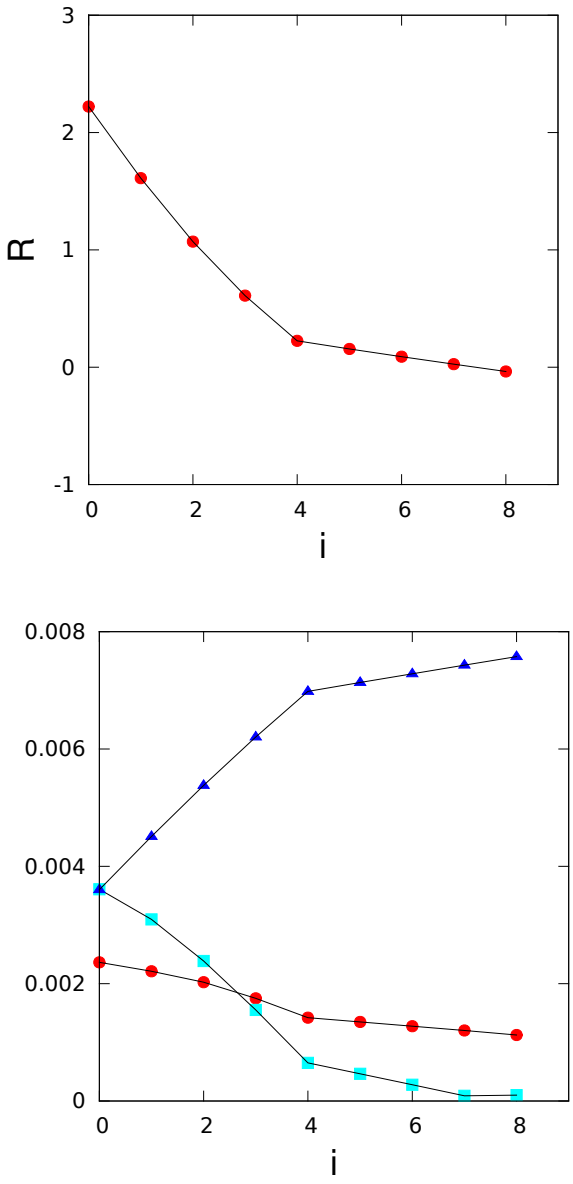


FIG. 10. Top plot: the ratio R [see Eq. (43)], as a function of the iteration step i, for a configuration, with lattice volume 48^4, that is a possible candidate for an element of the common boundary $\partial\Omega \cap \partial\Lambda$. (Note the small range of values on the y axis when compared to the corresponding plot in Fig. 9.) Bottom plot: the second smallest (non-trivial) eigenvalue λ_2 (full circles), the absolute value of the third derivative of the minimizing function $|\mathcal{E}'''|$ (full squares) and the fourth derivative of the minimizing function $\mathcal{E}''''$ (full triangles) as a function of the iteration step i, for the same configuration considered in the top plot. Here we used the gauge-fixing prescription *fc* (see Section III). In all cases the solid line is only to guide the eye.

On the other hand, for a few configurations[23] we found a very small value for the ratio R, also when the configuration is very close to $\partial\Omega$ (see Figure 10). In all these cases the absolute value of the third derivative $\mathcal{E}'''$ of $A_\mu(x)$ is much smaller (typically by a factor of order of 20) compared to the average (absolute) value obtained for the other configurations with the same lattice volume, thus forcing the value of R to stay small along the path $\tau_i A_\mu(x)$. Let us recall that a null value for $\mathcal{E}'''$ is indicative [4, 32] of a configuration belonging to the common boundary[24] of the first

[23] More exactly, for eleven configurations (out of a total of 530) the value of $|R|$ was smaller than 10 immediately before crossing the Gribov horizon and immediately after the crossing.

[24] This observation clarifies why it is important to consider at least a fourth-order Taylor expansion in the analysis of the minimizing

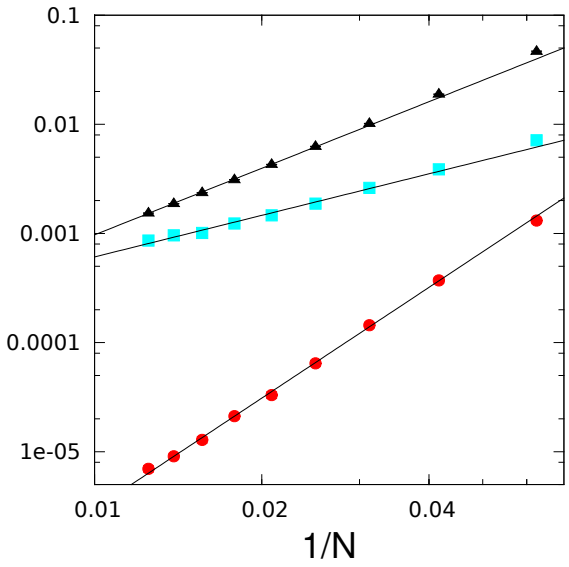


FIG. 11. The inverse ghost propagator $1/G(p_{min})$ (full triangles), evaluated at the smallest nonzero momentum p_{min}, the smallest nonzero eigenvalue λ_1 (full squares) and the lower-bound estimate in Eq. (32) (full circles) as a function of the inverse lattice size $1/N$. We also show, for each quantity, the fit to the function c/N^{η} (see discussion in the text). Here we used the gauge-fixing prescription *fc* (see Section III). All quantities are in lattice units. Note the logarithmic scale on both axes. The data points represent averages over gauge configurations, error bars correspond to one standard deviation. (We consider the statistical error only.)

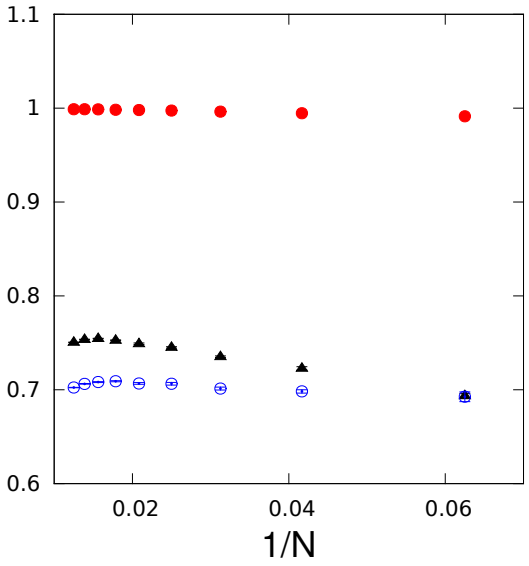


FIG. 12. The normalized horizon function h (empty circles), the Gribov ghost form-factor σ evaluated at the smallest nonzero momentum p_{min} (full triangles) and the upper bound ρ (full circles) as a function of the inverse lattice size $1/N$. Here we used the gauge-fixing prescription *fc* (see Section III). All quantities are in lattice units. The data points represent averages over gauge configurations, error bars correspond to one standard deviation. (We consider the statistical error only.)

---

function $\mathcal{E}$ (see for example Appendix A.1 in Ref. [31]). Indeed, the first derivative of $\mathcal{E}$ is null for all the configurations in Ω. At the same time, its second derivative is zero for configurations belonging to $\partial\Omega$ and the third derivative is also zero when one considers the common boundary of Ω and Λ. More precisely, one can show (see Refs. [61, 62]) that if $\mathcal{E}'''[A] \neq 0$ for $A \in \partial\Omega$, then the configuration $(1-s)A \in \Omega$, with $0 \leq s$ and s sufficiently small, cannot be an absolute minimum, i.e. $(1-s)A \notin \Lambda$.

Gribov region Ω and of the fundamental modular region Λ. These configurations, characterized by a small value of R for all factors τ_i, are therefore good candidates to belong to $\partial\Omega \cap \partial\Lambda$.

Using the above results we can now easily verify the new bound (32). Indeed, for each configuration $A_\mu(x)$, we can consider[25]

$$A'_\mu(x) \,=\, \widetilde{\tau}\, A_\mu(x) \,\equiv\, \frac{\tau_{n-1} + \tau_n}{2}\, A_\mu(x) \tag{44}$$

as a candidate for a configuration on the boundary of Ω, since $\tau_{n-1} A_\mu(x) \in \Omega$ and $\tau_n A_\mu(x) \notin \Omega$. Equivalently, with the notation of the previous section, we can write

$$A_\mu(x) \,=\, \rho\, A'_\mu(x)\;, \tag{45}$$

with $\rho = 1/\widetilde{\tau} < 1$, and the bound (32) becomes

$$\lambda_1 \left[\, \mathcal{M}[A] \,\right] \,=\, \lambda_1 \left[\, \mathcal{M}[\rho A'] \,\right] \,\geq\, (1-\rho)\, p^2_{min} \,=\, \left(1 - \frac{1}{\widetilde{\tau}}\right)\, p^2_{min}\;. \tag{46}$$

This last result is checked numerically in Figure 11. In the same figure, we show the inverse of the ghost propagator evaluated ad the smallest nonzero momentum p_{min}. As before, we see that λ_1 approaches $1/G(p_{min})$ at large volumes. On the other hand, the lower bound $(1-\rho)\, p^2_{min}$ seems to decrease faster than $1/G(p_{min})$. Indeed, if one tries to fit the data (see again Figure 11) using the fitting function c/N^η, the value for the exponent η is given[26] by $\eta \approx 2.0$ for the inverse ghost propagator, $\eta \approx 3.4$ for the lower bound $(1-\rho)\, p^2_{min}$ and by $\eta \approx 1.3$ for λ_1. This last result is in disagreement with the results presented in [10], where λ_1 displayed an exponent slightly larger than two (using significantly smaller lattice volumes and the so-called *best copy* average), and only in qualitative agreement with Ref. [36], where we found $\lambda_1 \sim L^{-1.53}$ (using, however, mostly data in the strong-coupling regime). [Here $L = aN$ is the physical size of the lattice.] One should also note that, since the above fits give $1/G(p_{min}) < \lambda_1$ for large values of N, simulations at larger lattice volumes are necessary in order to see how the inequality $1/G(p_{min}) \geq \lambda_1$ is realized in the infinite-volume limit.

As for the inequality (32), one should stress that it becomes an equality only when the eigenvectors corresponding to the smallest nonzero eigenvalues of the two matrices on the r.h.s. of Eq. (30) coincide. Thus, the fact that the new bound is very far from being saturated tells us that the eigenvector ψ_1 is very different from the plane waves corresponding to the smallest eigenvalue of the (lattice) Laplacian. That this is indeed the case can also be seen from the very small values obtained (for all configurations and Gribov copies) for the average projection $\overline{\psi}_1(p_{min})$ (see Figure 3).

Finally, in Figure 12 we check the inequalities (35) and (42), i.e.

$$\sigma(p_{min}),\, h \,\leq\, \rho\;. \tag{47}$$

To this end, the normalized horizon function h has been evaluated using Eq. (3.12.b) in Ref. [32] (see Ref. [18] for details of the numerical evaluation of h). One clearly sees that these inequalities are verified, for all values of the lattice size N. Moreover, $\sigma(p_{min})$ and h appear to stay far away from their upper bound $\rho \approx 1$. At the same time, one sees from the plot that $\sigma(p_{min}) \approx h$ at small volume. On the other hand, in the infinite-volume limit, the value of $\sigma(0)$ does not seem to agree with the value of h. This small disagreement, in contradiction with the result of Ref. [54], could be related to different finite-lattice-spacing effects,[27] in which case the observed difference should disappear in the continuum limit, and/or to possible non-perturbative contributions to these two quantities, since the proof in Ref. [54] is valid at the perturbative level.

---

[25] Since $\tau_n = \delta \tau_{n-1}$ and $\delta = 1 + \epsilon$ with $\epsilon \ll 1$, the definition $\widetilde{\tau} \equiv (\tau_{n-1} + \tau_n)/2$ is numerically equivalent (up to order ϵ) to the definition $\widetilde{\tau} \equiv \sqrt{\tau_{n-1}\, \tau_n}$.

[26] For these fits we considered only the data with $N > 16$.

[27] We include in these effects the dependence on the lattice spacing a introduced by the renormalization conditions for the considered quantities.

N	*fc*		*sfc*		*afc*		*bc*	
16	0.0248(8)	5.6 %	0.0245(8)	4.6 %	0.0240(8)	5.6 %	0.029(1)	5.4 %
32	0.023(2)	5.5 %	0.021(2)	7.5 %	0.022(2)	7.0 %	0.020(2)	7.0 %
48	0.026(4)	10.0%	0.023(3)	13.0%	0.019(2)	9.0 %	0.029(5)	14.0%
64	0.019(4)	20.0%	0.018(4)	20.0%	0.029(5)	20.0%	0.035(8)	10.0%

TABLE II. The average value of $|\mathcal{E}'''|$ and the percentage of configurations that are "very close" to the common boundary $\partial\Omega \cap \partial\Lambda$, i.e. with a value of $|\mathcal{E}'''|$ smaller than 1/20 of the corresponding average value, for each lattice volume and for the four types of gauge-fixing prescription considered (see Section III). The data represent averages over gauge configurations, errors correspond to one standard deviation. (We consider the statistical error only.)

VI. THE INFINITE-VOLUME LIMIT

In order to interpret the new bound (32) we recall that a distance function δ_l on SU(N_c) lattice configurations can be defined (see Appendix A in Ref. [32]) as

$$\delta_l^2(U,W) \,=\, \frac{1}{d\,V\,N_c} \sum_{\mu,x} \mathrm{Tr}\,\left\{ [U_\mu(x) - W_\mu(x)]^\dagger\ [U_\mu(x) - W_\mu(x)] \right\}\,, \tag{48}$$

where $U_\mu(x)$ and $W_\mu(x)$ are elements of the gauge group and † indicates the conjugate transpose matrix. Similarly, in the continuum, we can write

$$\delta_c^2(A,B) \,=\, \frac{1}{d\,V\,(N_c^2-1)} \sum_{\mu,x} \mathrm{Tr}\,\left\{ [A_\mu(x) - B_\mu(x)]^\dagger\ [A_\mu(x) - B_\mu(x)] \right\}\,, \tag{49}$$

where $A_\mu(x)$ and $B_\mu(x)$ are now elements of the algebra generating the gauge group. Both definitions are invariant with respect to global and to local gauge transformations,[28] i.e. $\delta_l^2(U^g,W^g) = \delta_l^2(U,W)$ for a general gauge transformation g [and similarly for $\delta_c^2(A,B)$]. Then, if $B = \rho A$ and $\rho \in \Re$, we have

$$\delta_c^2(A,B) \,=\, \frac{(1-\rho)^2}{d\,V\,(N_c^2-1)} \sum_{\mu,x} \mathrm{Tr}\,\left\{ A_\mu(x)^\dagger\, A_\mu(x) \right\} \,=\, (1-\rho)^2\ \|A\|^2\,, \tag{50}$$

where

$$\|A\|^2 \,\equiv\, \frac{1}{d\,V\,(N_c^2-1)} \sum_{\mu,x} \mathrm{Tr}\,\left\{ A_\mu(x)^\dagger\, A_\mu(x) \right\} \,=\, \frac{1}{d\,V\,(N_c^2-1)} \sum_{\mu,x,b} |\,A_\mu^b(x)|^2 \tag{51}$$

is the (average) norm square of the components of the gauge field. Therefore, following the notation of the previous section, i.e. considering a configuration $A' \in \partial\Omega$ and a configuration $B = \rho A' \in \Omega$, with $\rho \in [0,1]$, we have from (49) that

$$\rho \,=\, \sqrt{\frac{\delta_c^2(0,\rho A')}{\|A'\|^2}}\,. \tag{52}$$

This means that the factor ρ can be viewed as a normalized distance of the configuration $B = \rho A'$ from the "origin" $A = 0$, along a direction parallel to A'. Equivalently, the factor $1-\rho$ in Eq. (31) is a normalized distance of the configuration $\rho A'$ from the boundary of the region Ω (along the same direction).[29] The inequality (32) is therefore a simple mathematical realization of the intuitive statement that the behavior of λ_1 in the infinite-volume limit is

---

[28] If the configurations $U_\mu(x), W_\mu(x)$ [or $A_\mu(x), B_\mu(x)$] belong to the same gauge orbit, this invariance indicates that the distance between the two configurations is independent of the "choice of the origin" for the given orbit.

[29] Let us note that the dependence of the FP eigenvalues on the distance of the configuration from the first Gribov horizon has been considered in Ref. [63] within a perturbative study of the FP spectrum.

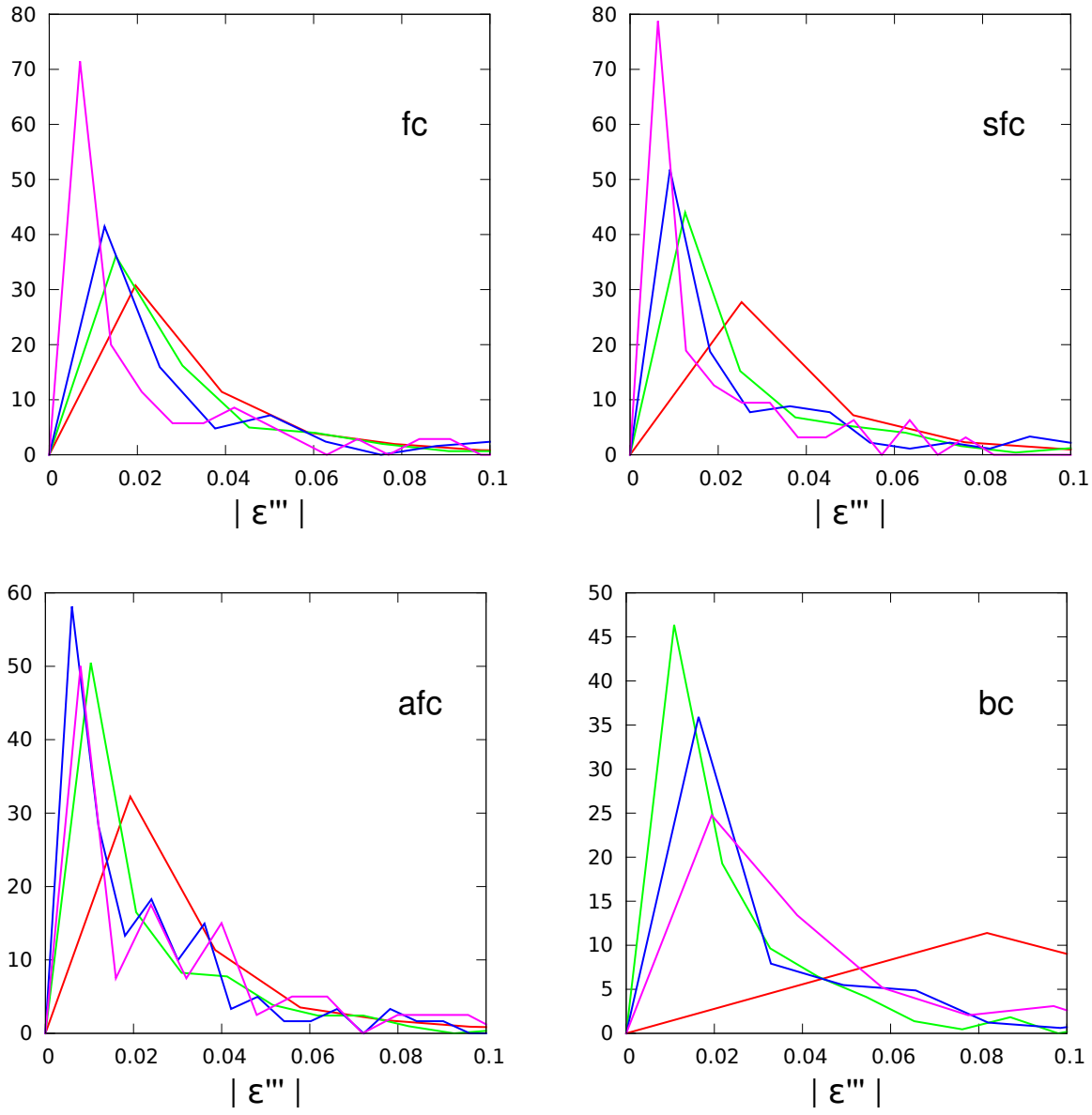


FIG. 13. Histogram distribution of $|\mathcal{E}'''|$ for the lattice sizes $N = 16$ (red line), 32 (green line), 48 (blue line) and 64 (magenta line) using 20 bins. The area of the histograms is normalized to 1. In order to reveal the distribution of the data with a small value of $|\mathcal{E}'''|$, we show only the interval $[0, 0.1]$. Four types of gauge-fixing prescription are considered (see Section III): *fc* (upper left plot), *sfc* (upper right plot), *afc* (lower left plot) and *bc* (lower right plot).

controlled by the speed at which an average thermalized and gauge-fixed configuration approaches the boundary $\partial\Omega$ (see discussion in the Introduction).

The new bounds give us useful and quantitative insights into the realization of the infinite-volume limit in the ghost sector. In particular, one can easily prove some generally accepted facts about the Gribov-Zwanziger confinement scenario. For example, a simple consequence of the inequality (32) is that if, in the infinite-volume limit, the functional integration gets concentrated in a region (strictly) inside Ω, then we have $1 - \rho > 0$ and the ghost propagator will

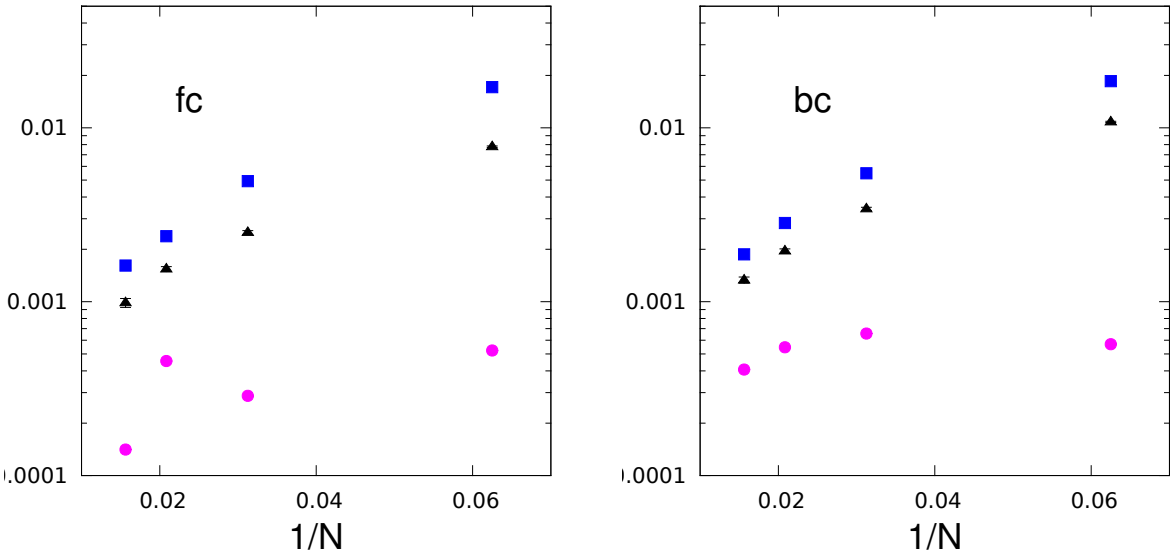


FIG. 14. The largest (full squares), the smallest (full circles) and the average value (full triangles) of the smallest nonzero eigenvalue λ_1 as a function of the inverse lattice size $1/N$. All quantities are in lattice units. Two types of Gribov copies are considered (see Section III): *fc* (left plot) and *bc* (right plot). Similar results have been obtained for the sets of Gribov copies indicated with *sfc* and *afc*. Note the logarithmic scale on the y axis. Error bars around the average value of λ_1 correspond to one standard deviation. (We consider the statistical error only.)

display a tree-level behavior $\sim 1/p^2$ in the infrared region.[30] This observation is relevant when the theory is defined in the fundamental modular region Λ (what is sometimes called the absolute Landau gauge [26, 28]). Indeed, we know that $\Lambda \subset \Omega$ [52] and that the boundaries $\partial\Lambda$ and $\partial\Omega$ of these two regions have common points [62]. Then, we can immediately conclude, for the absolute Landau gauge and in the limit of infinite volume, that a measure concentrated on the common boundary of Λ and Ω is a necessary condition for an infrared-enhanced ghost propagator. At the same time, one can infer some interesting implications from published data. Indeed, the same line of reasoning and the fact that the lower bound of the so-called b-corridor displayed in Figure 3 of Ref. [28] is essentially flat tell us that (at least for relatively small lattice volumes) it is always possible to find Gribov copies very far away from $\partial\Omega$.

Using the results presented in the previous section, i.e. looking at the data for the third derivative $\mathcal{E}'''$ of the minimizing function,[31] one can also try to estimate the percentage of configurations that are "very close" to the common boundary $\partial\Omega \cap \partial\Lambda$. To this end we evaluated the average value of $|\mathcal{E}'''|$. One notices (see Table II) that the results obtained are more or less independent of the lattice size N and of the type of Gribov copy considered, with values displaying small fluctuations around 0.024. We also checked how many configurations are characterized by a value of $|\mathcal{E}'''|$ smaller than one twentieth of the corresponding average value. As one can see from the same Table, as the lattice size increases there is a noticeable increase in the percentage of configurations that are good candidates for the common boundary $\partial\Omega \cap \partial\Lambda$. At the same time, by looking at the distribution of the values of $|\mathcal{E}'''|$ (see Figure 13) we find that, for the *fc* and *sfc* gauge-fixing choices, the distribution gets strongly concentrated below the value 0.01 as the lattice size N increases. On the other hand, for the *afc* and *bc* gauge-fixing choices, i.e. for configurations that are "closer" to the fundamental modular region Λ, the behavior of the peak of the distribution is not monotonically decreasing with N. Of course, in the case of $N = 48$ and 64, the number (only 100 or 50) of data points may be insufficient to sample correctly the distribution of $|\mathcal{E}'''|$ and to produce a reliable 20-bin histogram. Thus, these results should be verified by considering larger sets of data and (possibly) larger lattice volumes.

[30] See also the discussion in Sec. 4.1 of Ref. [4].
[31] Here and below we used for the analysis the same set of configurations considered in Section III.

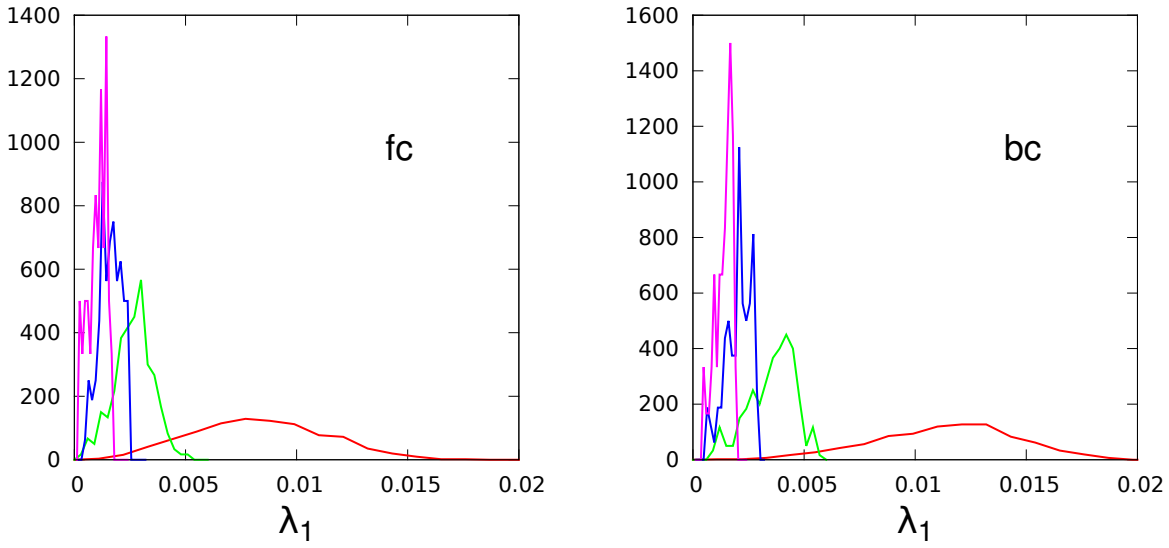


FIG. 15. Histogram distribution of the smallest nonzero eigenvalue λ_1 for the lattice sizes $N = 16$ (red line), 32 (green line), 48 (blue line) and 64 (magenta line) using 20 bins. The area of the histograms is normalized to 1. Two types of Gribov copies are considered (see Section III): *fc* (left plot) and *bc* (right plot). Similar results have been obtained for the sets of Gribov copies indicated with *sfc* and *afc*.

In order to study the infinite-volume limit in more detail, we can now follow Refs. [10, 13] and consider the distribution of the smallest nonzero eigenvalue λ_1 as a function of the lattice size (see Figures 14 and 15). In particular, from Figure 14 it is clear that the average value of λ_1, as well as its largest value, are monotonically decreasing as the lattice size increases, for the four types of statistics considered here. Conversely, its smallest value shows in some cases a non-monotonic behavior. At the same time, from Figure 15, one sees that the distribution of λ_1 changes considerably when going from $N = 16$ to $N = 32$. Indeed, in the former case, one has a very broad distribution for the smallest nonzero eigenvalues, with long tails (compared to the central value), while in the latter case we already see a more concentrated distribution[32] for the values of λ_1. The same relatively small spread for the values of λ_1 is seen for $N = 48$ and 64. Thus, results obtained at small lattice volumes are strongly affected by how well (or badly) the tails of the λ_1-distribution is sampled. Indeed, for small volumes we expect the thermalized and gauge-fixed configuration to belong to the center of the distribution in most of the cases. On the other hand, occasionally, one can obtain a configuration in the long tails of the distribution and, in particular, one that strongly feels the effects of $\partial\Omega$ or, equivalently, a configuration for which the inequality (32) approaches an equality. This observation supports and explains results obtained by various groups for the so-called exceptional configurations, found in the ghost sector of Landau gauge [9, 10, 19, 22, 26, 64, 65] and of Coulomb gauge [66–69]. Indeed, it seems clear that the presence of these exceptional configurations

- increases with the coupling β [19], i.e. when the physical lattice volume is typically smaller;
- decreases when the statistical average is constrained to the fundamental modular region [22], i.e. when the values of λ_1 are typically larger (compare the *bc* average to the *fc* average in Figures 14 and 15);
- is not correlated to anomalous values of the Polyakov loop and to "toron" excitations [19];
- is correlated to very small values of the smallest nonzero eigenvalue of the FP matrix [13, 66–69] or, equivalently, to large contributions to the ghost propagator [10, 22];

[32] These results are in qualitative agreement with Figure 1 of Ref. [10].

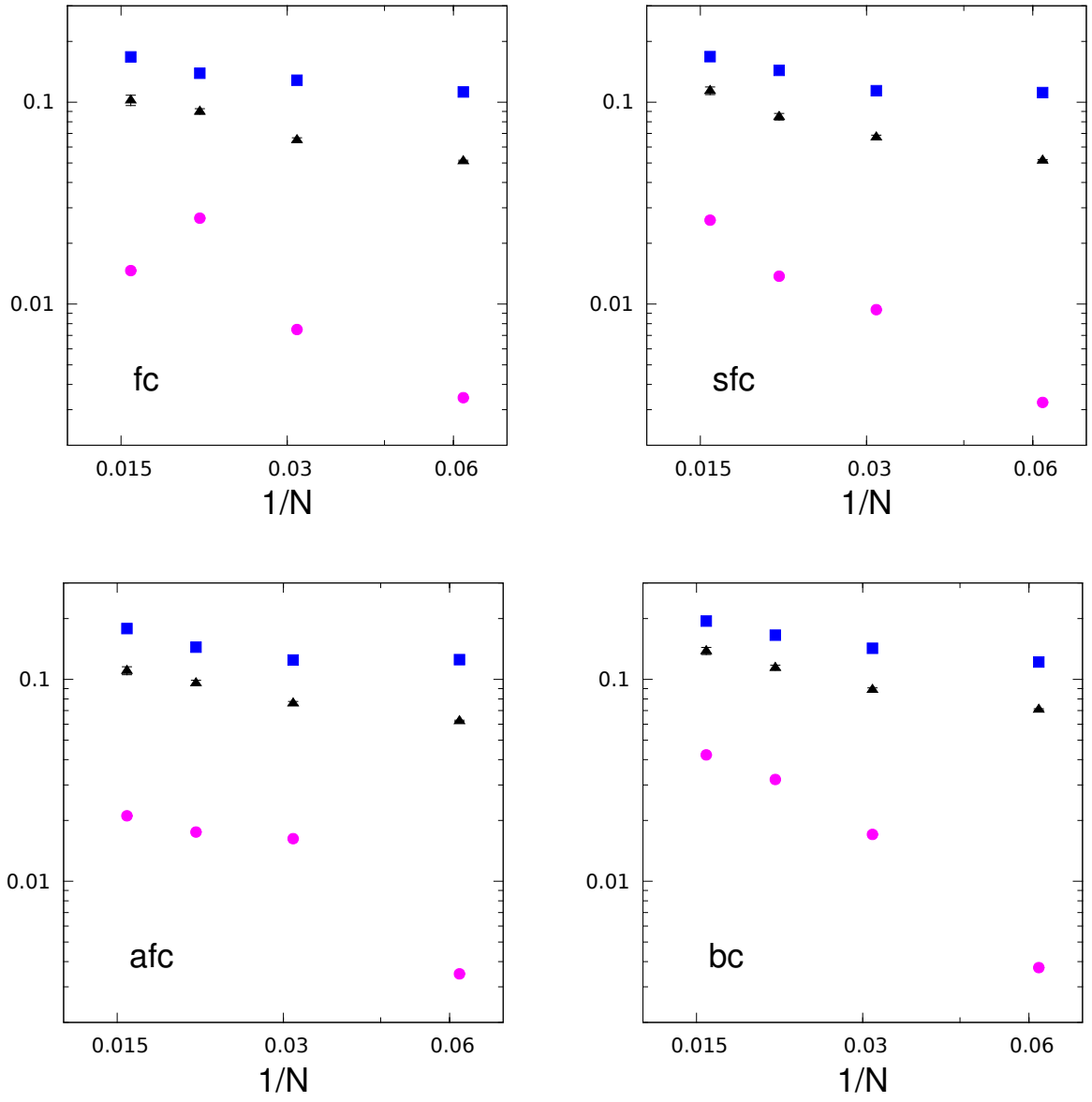


FIG. 16. The largest (full squares), the smallest (full circles) and the average value (full triangles) of the smallest nonzero eigenvalue λ_1, all divided by the smallest nonzero momentum squared p^2_{min}, as a function of the inverse lattice size $1/N$. All quantities are in lattice units. Four types of gauge-fixing prescription are considered (see Section III): *fc* (upper left plot), *sfc* (upper right plot), *afc* (lower left plot) and *bc* (lower right plot). Note the logarithmic scale on both axes. Error bars around the average value of λ_1/p^2_{min} correspond to one standard deviation. (We consider the statistical error only.)

- depends on the "direction" of the momentum p used to evaluate the ghost propagator — i.e. rotational invariance is broken [22] — since the smallest eigenvalue of the (lattice) Laplacian, entering the new bound (32), is d-fold degenerate (in the d-dimensional case);
- is correlated to very long minimization processes of the numerical gauge fixing [9, 26, 68], since the structure of the gauge orbit becomes more complicated near $\partial\Omega$ (see for example Figures 1 and 2 in [62] and Figure 2 in [18]), with the presence of various stationary points and flat directions.

Let us note that different approaches have been considered in the literature for dealing with these anomalous configurations. For example, in Coulomb gauge, the evaluation of the Coulomb potential [66, 67, 69] — which involves two

powers of the inverse FP matrix — and of the ghost propagator [68] is usually done by taking these configurations out of the statistical average. On the other hand, since the anomalous behavior in the ghost sector is not rotationally invariant, the authors of Ref. [22] suggested to average the data over different realizations of the same momentum p, in order to reduce the systematic effects due to these exceptional configurations. Finally, in Refs. [64, 65], the authors observed that using only the exceptional configurations can give results in a better agreement with the scaling solution [57–60] of the Dyson-Schwinger equations.

More recently, exceptional configurations have been viewed [13, 28, 33] as representatives in the implementation of minimal Landau gauge with additional conditions. Such gauge choices are introduced mainly as a possible lattice realization[33] of the scaling solution and of the one-parameter family [71–74] of the so-called massive solutions [75–79] (see also Refs. [53, 80–87] for other approaches and points of view on the scaling and/or the massive solutions).

Considering again the inequality (32), we also see that, from the numerical point of view, the ratio $\lambda_1[\,\mathcal{M}[A]\,]/p^2_{min}$ can be used as an upper-bound estimate of the distance $1-\rho$ of a configuration A from the boundary $\partial\Omega$. It is therefore interesting to rescale the data presented in Figure 14 for the smallest nonzero eigenvalue λ_1 by $1/p^2_{min}$. The results are shown in Figure 16. It seems that, for the four types of statistics considered in this work, this upper bound increases in the large-volume limit, i.e. λ_1 goes to zero more slowly than $p^2_{min} \sim 1/N^2$. Of course, since the ratio $\lambda_1[\,\mathcal{M}[A]\,]/p^2_{min}$ is an upper bound for $1-\rho$, this result does not imply that the quantity ρ does not go to 1 in the infinite-volume limit, as indeed seems to be the case (at least for the *fc* average, see the plot in Figure 12).

We plan to extend our numerical simulations in the near future. In particular, since we did not do an extensive search of Gribov copies as in Refs. [13, 28, 33], our results apply, for the moment, only to the four types of statistics considered here. On the other hand, one should recall that a systematic search of lattice Gribov copies is numerically very difficult, already for very small lattice volumes [88], and that some of the lattice copies are just lattice artifacts, as in the compact $U(1)$ case.

VII. CONCLUSIONS

In this section we sum up the main results presented in this work. Considering the various bounds proven in the text and their numerical verification, we can say that:

1. The bound (32) allows a simple mathematical realization of the assumptions considered in the Introduction. It connects non-Abelian aspects of Yang-Mills theory in Landau gauge to a simple geometrical parameter ρ, which can be interpreted as a normalized distance of a configuration A in the Gribov region Ω from the origin $A=0$. (Equivalently, $\rho^{-1}A$ is a configuration on the boundary $\partial\Omega$ of Ω.)

2. In the infinite-volume limit one finds $\lambda_1 \approx \lambda_2$, as expected. On the other hand, this equality is approached quite slowly by the lattice data. Indeed, when going from $N=16$ to $N=64$ (for $\beta=2.2$) we see that the ratio λ_1/λ_2 changes from about 0.7 to about 0.78, for the four types of statistics considered here.

3. As the lattice size increases, it seems easier to find candidate configurations for the common boundary $\partial\Omega \cap \partial\Lambda$. These are anomalous lattice configurations characterized by a very small absolute value for the third derivative of the minimizing functional along the direction of ψ_1, the eigenvector corresponding to the smallest nonzero eigenvalue λ_1.

4. For large lattice sizes N the relations

$$G(p_{min}) \;\approx\; \frac{1}{\lambda_1} \;<\; \frac{1}{p^2_{min}\;(1-\rho)} \tag{53}$$

are satisfied by lattice data in minimal Landau gauge.

---

[33] See Ref. [70] for various possible criticisms to this interpretation.

5. Since the two upper bounds (2) and (14) are almost saturated by our data, we conclude that $\lambda_i \approx \lambda_1$ [see comment below Eq. (9)]. This constitutes a numerical verification of the statement that "all horizons are one horizon", discussed in Section 3 of Ref. [4].

6. Since the lower bounds (2), (10) and (32) are far from being saturated by the lattice data, we can say that, for a generic configuration, the eigenvector ψ_1 is very different from the plane waves corresponding to the eigenvalue p^2_{min} of (minus) the lattice Laplacian.

7. The smallest nonzero eigenvalue λ_1 of the FP matrix goes to zero more slowly than $1/N^2$ for the four types of statistics considered here, supporting the so-called massive solution of the Dyson-Schwinger equations.

8. The lower bound $p^2_{min}\,(1-\rho)$ goes to zero as $1/N^\eta$ with η reasonably larger than 2, at least for the *fc* gauge-fixing prescription. Moreover, even for small lattice volumes, the value of ρ is very close to 1, i.e. most lattice configurations are indeed very close to the first Gribov horizon $\partial\Omega$.

Observations 4, 5 and 6 above explain why it is "difficult to find" a scaling solution on the lattice. Indeed, our data suggest that configurations producing an infrared-enhanced ghost propagator should almost saturate the new bound (32), i.e. their eigenvector ψ_1 should have a large projection on at least one of the plane waves corresponding to p^2_{min}. In this case, λ_1 would go to zero faster than $1/N^2$ and one would also find the value of the ghost propagator $G(p_{min})$ to be mostly given by the first term of the sum (4), i.e. the lower bound (2) would be almost saturated. On the other hand, this would contradict the intuitive picture that, in the infinite-volume limit: i) the spectrum of the FP matrix should become continuous (see Observation 2 above) and ii) the eigenvalue *density* around $\lambda \sim 0$ should be relevant for the IR behavior of $G(p)$. Moreover, this would imply that nonperturbative effects, such as color confinement, be driven by configurations whose FP matrix $\mathcal{M}$ is "dominated" by an eigenvector ψ_1 very similar to the corresponding eigenvector of $\mathcal{M} = -\partial_\mu\partial^\mu$, i.e. to ψ_1 of the free case! In this sense we agree with the observation made in the Conclusions of Ref. [87] that it is very difficult (if not impossible) to find a scaling solution on the lattice.

The above considerations also answer the question posed in Ref. [87]: which are the "appropriate boundary conditions" for a lattice configuration in order to find a scaling solution in Monte Carlo simulations of Yang-Mills theory? Indeed, we believe that the above discussion clarifies the properties of a "would-be typical lattice-scaling configuration", which, up to now, was defined only operationally [28, 33]. At the same time, Observation 8 seems to disprove the conjecture of Ref. [87] that "the scaling solution is related to the formation of the Gribov horizon". In fact, since essentially all lattice configurations, even for $N = 16$, are very close to $\partial\Omega$, it seems to us that it is not enough to have a Gribov horizon in order to produce a scaling solution. On the contrary, the key ingredient is *how* this boundary is encoded in the FP matrix.

From the analytic point of view, if one desires to isolate configurations displaying a scaling behavior, the simplest candidates for which ψ_1 is almost a plane wave are probably Abelian configurations, since in this case it might be easier to minimize the contribution of the operator $K[A]$ to the eigenvalue λ_1. On the other hand, one should note that it is not enough to find specific examples of lattice configurations whose FP matrix satisfies the properties discussed above. One should also show that this type of minima exists for all (or almost all) gauge orbits, so that their contribution to the functional integration (or, equivalently, to a Monte Carlo sampling) can be relevant.

ACKNOWLEDGMENTS

We thank M. Chiapparini, M.S. Guimarães and S.P. Sorella for useful discussions. We acknowledge partial support from FAPESP **grant # 2009/50180-0** and from CNPq. We would like to acknowledge computing time provided on the Blue Gene/P supercomputer supported by the Research Computing Support Group (Rice University) and

Laboratório de Computação Científica Avançada (Universidade de São Paulo).

---

[1] A. Cucchieri and T. Mendes, arXiv:0809.2777 [hep-lat].
[2] A. Cucchieri and T. Mendes, PoS **CONFINEMENT8**, 040 (2008).
[3] A. Cucchieri and T. Mendes, PoS **QCD-TNT09**, 026 (2009).
[4] D. Zwanziger, Nucl. Phys. B **378**, 525 (1992).
[5] D. Zwanziger, Nucl. Phys. B **399**, 477 (1993).
[6] N. Vandersickel, arXiv:1104.1315 [hep-th].
[7] N. Vandersickel and D. Zwanziger, Phys. Rept. **520**, 175 (2012).
[8] A. Maas, Phys. Rev. D **75**, 116004 (2007).
[9] A. Cucchieri, A. Maas and T. Mendes, Phys. Rev. D **74**, 014503 (2006).
[10] A. Sternbeck, E. -M. Ilgenfritz and M. Müller-Preussker, Phys. Rev. D **73**, 014502 (2006).
[11] G. Damm, W. Kerler and V. K. Mitrjushkin, Phys. Lett. B **433**, 88 (1998).
[12] A. Cucchieri, [hep-lat/9908050].
[13] A. Sternbeck and M. Müller-Preussker, arXiv:1211.3057 [hep-lat].
[14] V. N. Gribov, Nucl. Phys. B **139**, 1 (1978).
[15] Y. L. Dokshitzer and D. E. Kharzeev, Ann. Rev. Nucl. Part. Sci. **54**, 487 (2004).
[16] R. F. Sobreiro and S. P. Sorella, hep-th/0504095.
[17] A. Cucchieri, Nucl. Phys. B **508**, 353 (1997).
[18] A. Cucchieri, Nucl. Phys. B **521**, 365 (1998).
[19] T. D. Bakeev, E. -M. Ilgenfritz, V. K. Mitrjushkin and M. Müller-Preussker, Phys. Rev. D **69**, 074507 (2004).
[20] P. J. Silva and O. Oliveira, Nucl. Phys. B **690**, 177 (2004).
[21] H. Nakajima and S. Furui, Nucl. Phys. Proc. Suppl. **141**, 34 (2005).
[22] A. Sternbeck, E. -M. Ilgenfritz, M. Müller-Preussker and A. Schiller, Phys. Rev. D **72**, 014507 (2005).
[23] A. Y. Lokhov, O. Pene and C. Roiesnel, hep-lat/0511049.
[24] I. L. Bogolubsky, G. Burgio, M. Müller-Preussker and V. K. Mitrjushkin, Phys. Rev. D **74**, 034503 (2006).
[25] I. L. Bogolubsky, V. G. Bornyakov, G. Burgio, E. M. Ilgenfritz, M. Müller-Preussker and V. K. Mitrjushkin, Phys. Rev. D **77**, 014504 (2008) [Erratum-ibid. D **77**, 039902 (2008)].
[26] A. Maas, Phys. Rev. D **79**, 014505 (2009).
[27] V. G. Bornyakov, V. K. Mitrjushkin and M. Müller-Preussker, Phys. Rev. D **79**, 074504 (2009).
[28] A. Maas, Phys. Lett. B **689**, 107 (2010).
[29] A. Maas, J. M. Pawlowski, D. Spielmann, A. Sternbeck and L. von Smekal, Eur. Phys. J. C **68**, 183 (2010).
[30] V. G. Bornyakov, V. K. Mitrjushkin and M. Müller-Preussker, Phys. Rev. D **81**, 054503 (2010).
[31] D. Zwanziger, Phys. Rev. D **69**, 016002 (2004).
[32] D. Zwanziger, Nucl. Phys. B **412**, 657 (1994).
[33] A. Maas, arXiv:1301.2965 [hep-th].
[34] V. G. Bornyakov, V. K. Mitrjushkin and R. N. Rogalyov, arXiv:1304.8130 [hep-lat].
[35] A. Cucchieri and T. Mendes, Phys. Rev. Lett. **100**, 241601 (2008).
[36] A. Cucchieri and T. Mendes, Phys. Rev. D **78**, 094503 (2008).
[37] D. Zwanziger, arXiv:1209.1974 [hep-ph].
[38] A. Maas and D. Zwanziger, arXiv:1301.3520 [hep-lat].
[39] J. Greensite, S. Olejnik and D. Zwanziger, JHEP **0505**, 070 (2005).
[40] J. C. R. Bloch, A. Cucchieri, K. Langfeld and T. Mendes, Nucl. Phys. B **687**, 76 (2004).
[41] A. Cucchieri and T. Mendes, Nucl. Phys. B **471**, 263 (1996).
[42] A. Cucchieri and T. Mendes, Nucl. Phys. Proc. Suppl. **53**, 811 (1997).
[43] J. E. Hetrick and P. de Forcrand, Nucl. Phys. Proc. Suppl. **63**, 838 (1998).
[44] G. S. Bali, V. Bornyakov, M. Müller-Preussker and K. Schilling, Phys. Rev. D **54**, 2863 (1996).
[45] P. Boucaud, J. P. Leroy, A. Le Yaouanc, A. Y. Lokhov, J. Micheli, O. Pene, J. Rodriguez-Quintero and C. Roiesnel, Phys. Rev. D **72**, 114503 (2005).
[46] *Lectures in basic computational numerical analysis*, J. M. McDonough (`www.engr.uky.edu/~acfd/egr537-lctrs.pdf`).

[47] T. Kalkreuter and H. Simma, Comput. Phys. Commun. **93**, 33 (1996).
[48] A. Cucchieri and T. Mendes, PoS LAT **2007**, 297 (2007).
[49] A. Cucchieri, D. Dudal, T. Mendes and N. Vandersickel, Phys. Rev. D **85**, 094513 (2012).
[50] *Matrix Algebra*, K. M. Abadir and J. R. Magnus (Cambridge University Press, New York, 2005).
[51] D. Zwanziger, Nucl. Phys. B **209**, 336 (1982).
[52] G. Dell'Antonio and D. Zwanziger, Commun. Math. Phys. **138**, 291 (1991).
[53] A. Cucchieri, D. Dudal and N. Vandersickel, Phys. Rev. D **85**, 085025 (2012).
[54] M. A. L. Capri, D. Dudal, M. S. Guimaraes, L. F. Palhares and S. P. Sorella, Phys. Lett. B **719**, 448 (2013).
[55] A. Maas, PoS QCD **-TNT-II**, 028 (2011).
[56] C. S. Fischer and J. M. Pawlowski, Phys. Rev. D **80**, 025023 (2009).
[57] L. von Smekal, A. Hauck and R. Alkofer, Annals Phys. **267**, 1 (1998) [Erratum-ibid. **269**, 182 (1998)].
[58] D. Zwanziger, Phys. Rev. D **65**, 094039 (2002).
[59] C. Lerche and L. von Smekal, Phys. Rev. D **65**, 125006 (2002).
[60] C. S. Fischer, J. Phys. G **32**, R253 (2006).
[61] M.A. Semenov-Tyan-Shanskii and V.A. Franke, *Zapiski Nauchnykh Seminarov Leningradskogo Otdeleniya Matematicheskogo Instituta im. V.A. Steklov AN SSSR* 120, 159 (1982). Translation: Journal of Soviet Mathematics (Plenum Press, New York), 1999 (1986).
[62] P. van Baal, Nucl. Phys. B **369**, 259 (1992).
[63] J. Greensite, Phys. Rev. D **81**, 114011 (2010).
[64] S. Furui and H. Nakajima, Phys. Rev. D **70**, 094504 (2004).
[65] S. Furui and H. Nakajima, Braz. J. Phys. **37**, 186 (2007).
[66] J. Greensite, Acta Phys. Polon. B **40**, 3355 (2009).
[67] J. Greensite and S. Olejnik, Phys. Rev. D **81**, 074504 (2010).
[68] G. Burgio, M. Quandt and H. Reinhardt, Phys. Rev. D **86**, 045029 (2012).
[69] J. Greensite, PoS **QCD-TNT-II**, 024 (2011).
[70] A. Cucchieri and T. Mendes, AIP Conf. Proc. **1343**, 185 (2011).
[71] P. Boucaud, J-P. Leroy, A. L. Yaouanc, J. Micheli, O. Pene and J. Rodriguez-Quintero, JHEP **0806**, 012 (2008).
[72] P. Boucaud, J. P. Leroy, A. Le Yaouanc, J. Micheli, O. Pene and J. Rodriguez-Quintero, JHEP **0806**, 099 (2008).
[73] C. S. Fischer, A. Maas and J. M. Pawlowski, Annals Phys. **324**, 2408 (2009).
[74] J. Rodriguez-Quintero, JHEP **1101**, 105 (2011).
[75] A. C. Aguilar, A. A. Natale and P. S. Rodrigues da Silva, Phys. Rev. Lett. **90**, 152001 (2003).
[76] A. C. Aguilar and A. A. Natale, JHEP **0408**, 057 (2004).
[77] A. C. Aguilar and J. Papavassiliou, JHEP **0612**, 012 (2006).
[78] D. Binosi and J. Papavassiliou, Phys. Rept. **479**, 1 (2009).
[79] A. C. Aguilar and J. Papavassiliou, Phys. Rev. D **81**, 034003 (2010).
[80] M. Frasca, Phys. Lett. B **670**, 73 (2008).
[81] D. Dudal, J. A. Gracey, S. P. Sorella, N. Vandersickel and H. Verschelde, Phys. Rev. D **78**, 065047 (2008).
[82] K. -I. Kondo, Phys. Lett. B **678**, 322 (2009).
[83] M. Tissier and N. Wschebor, Phys. Rev. D **82**, 101701 (2010).
[84] M. Tissier and N. Wschebor, Phys. Rev. D **84**, 045018 (2011).
[85] A. Weber, Phys. Rev. D **85**, 125005 (2012).
[86] M. R. Pennington and D. J. Wilson, Phys. Rev. D **84**, 119901 (2011).
[87] F. J. Llanes-Estrada and R. Williams, Phys. Rev. D **86**, 065034 (2012).
[88] C. Hughes, D. Mehta and J. -I. Skullerud, Annals Phys. **331**, 188 (2013).